Photochemical investigation of porphyrins for use in Dye Sensitized Solar Cells

A Thesis Submitted to the College of

Graduate Studies and Research

in Partial Fulfillment of the Requirements

for the Degree of Master of Science

in the Department of Chemistry

University of Saskatchewan

Saskatoon

By

Brook R. Danger

© Copyright Brook R. Danger, May 2012. All rights reserved.

PERMISSION TO USE

In presenting this thesis/dissertation in partial fulfillment of the requirements for a Postgraduate degree from the University of Saskatchewan, it is agreed that the Libraries of this University may make it freely available for inspection. I further agree that permission for copying of this thesis/dissertation in any manner, in whole or in part, for scholarly purposes may be granted by the professor or professors who supervised my thesis/dissertation work or, in their absence, by the Head of the Department of Chemistry or the Dean of the College of Graduate Studies and Research at the University of Saskatchewan. It is understood that any copying or publication or use of this thesis/dissertation or parts thereof for financial gain shall not be allowed without my written permission. It is also understood that due recognition shall be given to me and to the University of Saskatchewan in any scholarly use which may be made of any material in my thesis/dissertation.

Requests for permission to copy or to make other uses of materials in this thesis/dissertation in whole or part should be addressed to:

Head of the Department of Chemistry
University of Saskatchewan
Saskatoon, Saskatchewan, Canada

Abstract

As Dye Sensitized Solar Cells (DSSCs) have become a more prominent focus of the research being published on alternative energy sources it is important to consider basic principles that show promise for improving the energy conversion efficiency of these cells. By choosing and building a dye system carefully it is possible to promote a process called triplet-triplet annihilation (TTA) which involves the upconversion of two relatively low energy triplet excited molecules to produce one highly excited singlet molecule and a ground state molecule ($2\ T_1 \rightarrow S_n + S_0$ [n>1]). This process will give DSSCs the ability to take advantage of the photon-rich near infrared portion of the solar spectrum making them inherently more efficient than systems which cannot undergo TTA.

Two dye systems which show promise as TTA capable light harvesters are zinc tetraphenylporphyrin (ZnTPP) and tin(IV)-dichloro,tetraphenylporphyrin ($SnCl_2TPP$). The photophysical properties of ZnTPP are studied in its standard form as well as in its ligated form. Ligation of the central atom with nitrogen containing bidentate ligands (i.e. pyrazine, 4,4-bipyridine etc…) can have a profound effect on both the properties of the monomer as well as the aggregate behavior of solvated dyes and their interaction with each other. The properties of $SnCl_2TPP$ are also examined and in particular methods for the formation of stacked molecular columns as manipulation of interactions between the individual dyes can significantly impact their ability to undergo TTA.

Spectral data indicate that ligation of the ZnTPP leads to the formation of a short lived charge transfer state which greatly decreases the lifetime of the S_2 state while having little effect on the S_1 decay kinetics. It also shows that there is little or no formation of six-coordinate ZnTPP (i.e. doubly ligated) which makes the formation of stacked supramolecular structures very difficult. Data concerning the electrochemical synthesis and chemical synthesis of a $SnCl_2TPP$ based stack were inconclusive but show some promise that may give direction to future work.

Acknowledgments

First and foremost I would like to thank my supervisors Dr. Ron Steer and Dr. Ian Burgess without whom I would likely be a jobless biologist. Both of them have always looked to my interests above their own and supported me fully in all of my academic pursuits. Their patient training in both photochemistry and electrochemistry has allowed me to experience some of the best parts of science and I don't believe that I can adequately thank them enough for all of the knowledge and experience they've shared with me.

I would also like to thank the various group members (especially Sunish and Manisankar) and university staff (particularly Sophie, Jason, Garth, Cathy, Rick, Ronda, Brenda, Dwight, Devin, Ted and Blair) for all of their help with my work. Without their efforts it's probable that I would have spent so much time trying to build my experiments that I would still be on page one of this thesis.

Thank you to the Department of Chemistry and it's various faculty who have always been kind to me and willing to lend me their expertise where mine and that of my supervisors was lacking. It was nice when they would give me resources too because no phys chem lab has decent synthetic glassware.

I thank God for the rich and blessed life that I've had and all of the opportunities that I've been given. Though I sometimes feel a bit spoiled, when I look at the life I've had I wouldn't trade it for another.

Lastly I want to thank my loving family and charming girlfriend for all of their support and feigned interest in what I do. Their allowing me to ramble about my research while showing genuine bursts of excitement about giant lasers made my job a lot more fun on the days when sitting in a dark room watching a computer count photons just wasn't enough excitement.

Table of Contents

Abstract ii

Acknowledgments iii

Table of Contents iv

List of Tables viii

List of Figures ix

List of Abbreviations xi

1. Introduction

1.1 Energy needs and solar energy as an alternative source 1

1.2 Natural systems 2

1.3 Different types of solar cells 2

1.4 Implications of solar photon flux 5

1.5 Dye sensitized solar cells 7

1.5.1 Current efficiencies and limitations 8

1.5.2 System kinetics and inherent energy losses 10

1.6 Electron transfer and electronic energy transfer 13

1.7 Porphyrin photophysics 18

1.7.1 Absorption and fluorescence properties 18

1.7.2 Tuning dye photoproperties 20

1.7.3 Excited state lifetimes and electron injection kinetics 22

1.7.4 Triplet triplet annihilation 24

1.8 Energy gap law 27

1.9 Supramolecular porphyrin studies 28

1.10 Objectives 29

2. Experimental

2.1 General methods and materials 31

2.2 Electronic absorption spectra 31

2.2.1 Instrument schematics and properties 31

2.2.2 Data treatment 32

2.3 Emission spectra 32

2.3.1 Instrument schematics and properties 33

2.3.2 Data treatment 33

2.4 Time correlated single photon counting 34

2.4.1 Alignment procedures, instrument schematics and properties 34

2.4.2 Data acquisition 35

2.4.3 Data treatment 36

2.5 Spectroelectrochemistry 37

2.5.1 Cell design 37

2.5.2 Data acquisition 39

2.6 Synthesis 41

2.6.1 Materials used 41

2.6.2 Synthesis of porphyrin stacks 41

3. Results

3.1 ZnTPP studies 42

3.1.1 Steady state absorbance data 42

3.1.2 Steady state emission data 45

3.1.3 Time correlated single photon counting 47

3.1.4 Fluorescence upconversion data 49

3.2 $SnCl_2TPP$ studies 51

3.2.1 Synthesis results 51

3.2.2 Absorbance and Raman spectra 53

3.2.3 Emission spectra and lifetime measurements 58

4. Discussion

4.1 Factors determining energy transfer rates 60

4.2 General effects of ligation 60

4.3 Excited state dynamics of ligated species 63

4.4 Energetics of electron transfer 64

4.5 Synthesis of porphyrin stacks 66

4.6 Porphyrin viability 69

5. Summary and future work

5.1 Summary 71

5.2 Future Work 72

References **73**

Appendices **80**

A. Pyrazine-ZnTPP ligation spectra **81**

List of Tables

3.1 S_1 temporal fluorescence decay data 48

3.2 S_2 decay parameters for ligated ZnTPP 50

3.3 Raman band assignment of starting materials and products of electrochemical synthesis 56

3.4 S_1 lifetime data for $SnCl_2TPP$ and (SnTPPO)n (?) 59

4.1 Electron transfer parameters for Soret excited ZnTPP:L in toluene 65

List of Figures

1.1	Basic bulk heterojunction stacked cell schematic	4
1.2	General schematic of a DSSC	5
1.3	ASTM standard solar spectral irradiance	6
1.4	Record solar cell efficiencies	9
1.5	Energetic processes in a DSSC	11
1.6	Electron injection efficiencies	12
1.7	Electron transfer potential energy wells	15
1.8	Typical ZnTPP absorbance and emission spectra	18
1.9	Peripheral ligation effects on emission properties	21
1.10	Homomolecular TTA Jablonski diagram	25
2.1	PVC spectroelectrochemical cell	38
2.2	ITO spectroelectrochemical cell	39
3.1	ZnTPP absorption profiles with increasing [bipy]	43
3.2	Scatchard plot	44
3.3	ZnTPP emission profiles with increasing [bipy]	46
3.4	S_1 decay of ZnTPP and bipy system	47
3.5	S_2 decay and S_1 rise profiles for ZnTPP:bipy system	49
3.6	Electrochemical synthesis cyclic voltammogram	52
3.7	Synthesis before and after absorption spectra	54
3.8	Raman spectra of starting materials and synthesis product	55
3.9	Q and B band absorption changes after synthesis	57

3.10 S_1 and S_2 emission of $SnCl_2TPP$ and (SnTPPO)n (?) 59

4.1 S_1 and delayed S_2 emission of $SnCl_2TPP$ and ZnTPP 62

4.2 Corrected S_1 emission for ligated and unligated ZnTPP 66

4.3 Proposed oxygen bridged dimer structure 69

List of Abbreviations

ASTM	American Society for Testing and Materials
BHJ	bulk heterojunction
bipy	4,4'-bipyridine
CB	conduction band
CV	cyclic voltammogram
DSSC	dye sensitized solar cell
DW	Durbin-Watson
EGL	energy gap law
ET	electron transfer
FC	Franck-Condon factor
IEEE	Institute of Electrical and Electronics Engineers
IRF	instrument response function
ISC	intersystem crossing
ITO	indium-tin oxide
Jsc	short circuit current
NIR	near infrared
PMT	photomultiplier tube
PTI	Photon Technology International
SHG	second harmonic generator
$SnCl_2TPP$	tin(IV)-dichloro-tetraphenylporphyrin
THG	third harmonic generator
TTA	Triplet-triplet annihilation
Voc	open circuit potential
ZnTPP	zinc tetraphenylporphyrin

1. Introduction

1.1 Energy needs and solar energy as an alternative source

As the energy demands of the world continue to increase[1] and the availability of mainstream energy sources, namely hydrocarbon deposits, decreases[2] the development of alternative energy sources is becoming a pressing problem.

It is currently estimated that $5.32 \cdot 10^{17}$ kJ of energy are consumed globally every year.[1] The sun's energy that strikes the earth is estimated at $3 \cdot 10^{21}$ kJ per year, which would easily provide for current consumption if even only a small fraction of that energy could be collected[3]. It is unlikely that solar energy will be the only alternative energy source used to replace more conventional methods of energy production but it is a very dependable and extensive source of energy upon which we can draw. However, for solar to be viable a relatively good efficiency to cost of production ratio must be obtained. Current solar cell technology has achieved conversion efficiencies as high as 42%[4-5], which may be efficient enough to meet global energy demands but this has only been achieved in research devices.

The biggest distinction among current solar cell technologies is that of inorganic and organic solar cells. Organic cells are based on highly conjugated dyes which harvest light and pass their energy, via electron transfer, to an electrode while inorganic cells use doped semiconductors which directly harvest photons. The highest efficiency organic solar cells are rarely reproducible and there has yet to be one that can be efficiently mass produced that has an efficiency higher than ca. 6.5%. The only cells that currently show promise for low cost mass production are the bulk heterojunction type[6] . For this reason the most widely used solar cells are inorganic, single crystal silicon, which when mass produced have efficiencies of approximately 25%.[7] This is a relatively high efficiency but they are still too expensive to replace fossil fuels as an energy source even though prices for oil on the world market have maintained a reasonably high price. This means that either solar energy should be abandoned in search of other more viable sources or solar cells with a higher energy conversion efficiency to material/production cost ratio must be developed.

1.2 Natural systems

The photosynthetic systems found in nature have provided a good starting point for the production of viable solar energy harvesting systems. By studying their structures and applying the principles to synthetic systems it may be possible to create an optimal system. These systems are based around light harvesting by chromophores such as chlorophylls, xanthophylls and carotenoids which are arranged in antenna-like complexes radiating from a central reaction centre. These chromophores closely resemble a metallated (typically Mg) porphyrin system which has led to the use of similar metallated, highly conjugated porphyrinoids when looking for ideal absorbers. Once light has been absorbed by a chromophore the energy is quickly transferred among the chromophores and directed toward the reaction centre where charge separation occurs. The resultant electrochemical potential is used to drive various redox processes.[8-9] While many of these steps are not fully understood, natural systems may still hold promise for improving the current approach to photovoltaics.[10]

A recent paper shows that while the maximum theoretical efficiency of photosynthetic glucose production is 6.0%, when the thermodynamic limitations and energetic losses of the natural system are accounted for, a comparable photovoltaic cell (single junction semiconducting system) has a theoretical limit of approximately 24%.[11-13] Using current synthetic procedures, attaining an efficiency of that magnitude in a photovoltaic cell is an expensive and technically demanding process.[14] Fortunately advances in procedures and materials for the production of solar cells continue to increase the likelihood of creating an efficient and robust photovoltaic system that can be effectively mass produced.

1.3 Different types of Solar Cells

Three of the more common types of solar cells that are currently being studied by photovoltaic research groups will be introduced here to give a foundation for comparisons among different types of systems as well as a general understanding of individual systems so they can be further examined in later sections. These are systems which show promise in their ability to achieve

higher efficiencies (see section 1.5.1) at lower costs; they consist of dye sensitized solar cells (DSSC), bulk heterojunction (BHJ) and crystalline silicon solar cells.

As mentioned above, silicon solar cells are the most commercially available, due mainly to their reproducibly high efficiencies and relatively simple design, but they are quite costly to produce.[15] These solar cells function on the simple principle of an electron being photoexcited from the valence band of the semiconducting material to its conduction band. This process takes place at a p-n junction which can be adjusted by using different dopants and/or dopant concentrations to tune the band gap of the semiconductor. The p-n junction makes photoexcitation much easier while also regulating the direction of the flow of charge within the semiconductor helping to prevent energetic losses due to charge recombination.

Bulk heterojunction cells are an organic photovoltaic system that presents the most accessible means of production but also typically has the lowest efficiencies of the three types discussed here. BHJ cells typically consist of a somewhat uncontrolled combination of a polymer and a fullerene-containing compound sandwiched between a set of electrodes (figure 1.1). The polymer absorbs light and acts as an electron donor to the fullerene. This process is very efficient but only at the interface of the two types of layers, which is the reason for increasing the surface area of the interface by mixing the two layers. Once the electron has been accepted the fullerene layer acts as an electron conductor moving the excited electrons towards a metal (typically aluminum) electrode and the organic polymer acts as a hole conductor moving the holes toward a transparent indium-tin oxide (ITO) electrode, with an external load, completing the circuit. The nature of these cells makes it possible for large losses due to recombination of electrons and holes to take place at electrodes as it is possible for one type of material to be in contact with both electrodes. To avoid these losses layers of poly(3,4-ethylenedioxythiophene) poly(styrenesulfonate)are typically used to block the flow of electrons to the ITO electrode while still allowing diffusion of holes to the electrode. On the other side, titanium dioxide is used as a very efficient hole blocking material which will only allow electrons to access the Al electrode.[16-18] As seen in Figure 1.1 it is also possible to stack these cells in an effort to absorb

more of the incident light by using several organic materials that absorb at different wavelengths.

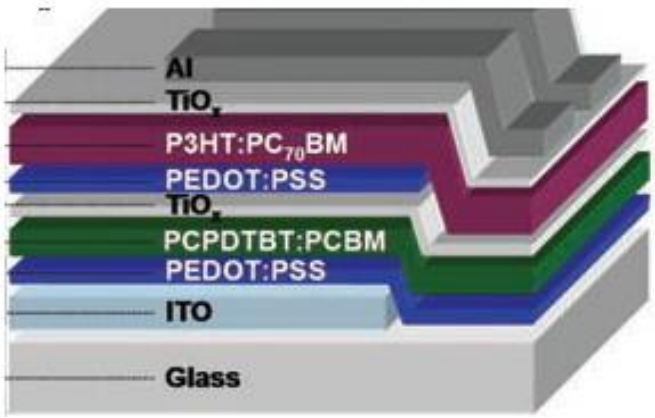

Figure 1.1 Basic BHJ setup of a stacked cell where two different organic layers are used to absorb more light.[19]

The ability to create these cells using simple techniques, as well as the ability to make flexible BHJ cells by using plastic substrates, has kept the interest in them strong even though their efficiencies are so low.[6]

DSSCs represent a type of middle ground between silicon and BHJ cells. Research cells have regularly attained efficiencies between 10 and 12% and they are relatively simple and inexpensive to construct when compared with the process of silicon solar cell production. Figure 1.2 shows the basic components of a general DSSC setup which is described in more detail here. A dye with particularly desirable photoproperties is chosen and attached, either through physisorption to the surface or chemical bonding via bridging tethers, to a transparent semiconducting surface which acts as an anode for the cell. Semiconducting nanoparticles are used to increase the surface area available for dye loading[20] but the preparation of these surfaces has been shown to have significant effects on the performance of the cell and is one source of irregularities in DSSCs.[21] Once electrons have passed through the external circuit of the cell, and done whatever electrical work the cell is intended to accomplish, charge is

conducted via a redox pair back to the dye radical cation where the original ground state is then regenerated.

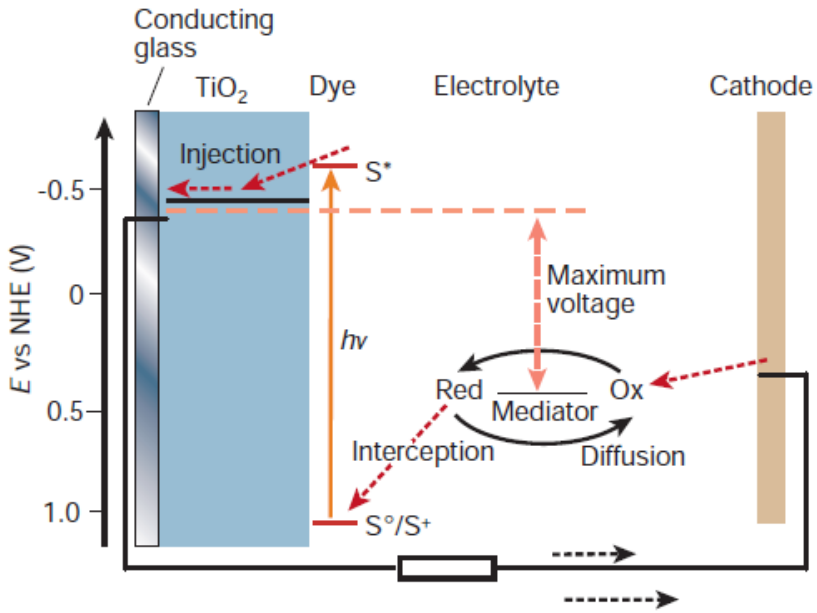

Figure 1.2 General schematic of a DSSC as originally conceived by M. Graetzel.[3]

1.4 Implications of solar photon flux

The energy harvested by photovoltaics must necessarily depend on the sunlight that is incident on the cell itself. For this reason certain locations will obviously be more advantageous for the implementation of photovoltaic energy harvesting but, regardless of the location of the cell, the ability to absorb more of the incident light will result in better overall performance. Figure 1.3 shows the solar spectral irradiance (a measure of the amount of power from the sun per nm bandwidth that strikes a given amount of surface area) under specific conditions (Air Mass [AM] 1.5, 37° tilted surface) on a cloudless day. The total integrated area of the graph gives a value of 1000.4 W m^{-2} and upon inspection it is clear that much of this power comes from light that falls in the red and infrared portion of the spectrum. In fact one third of the sun's power lies beyond 1000 nm.[22]

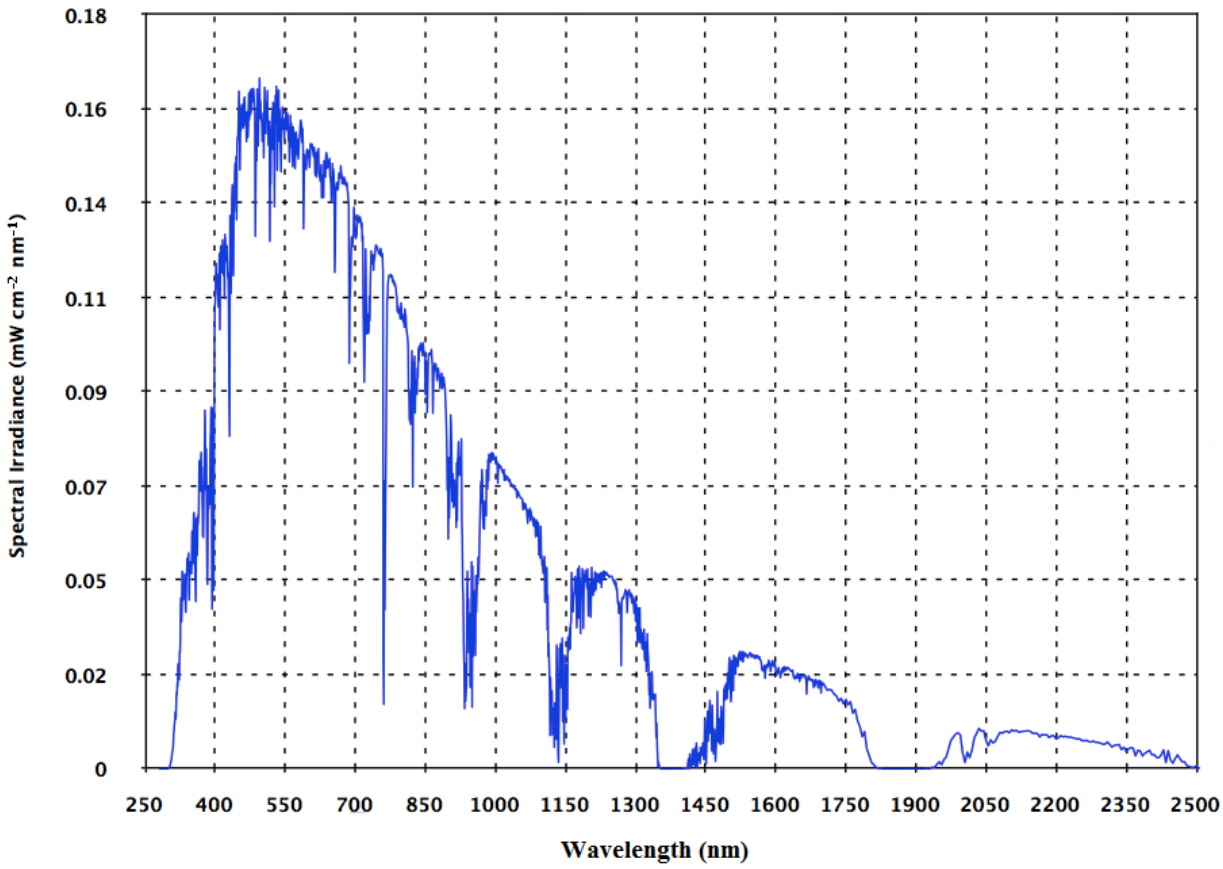

Figure 1.3 A.S.T.M. Standard G173-03 solar spectral irradiance for AM 1.5 and global tilt [23]

Most photovoltaic cells are unable to take advantage of the power that lies in these regions of the solar spectrum as the energy of the individual photons is too small to bridge the bandgap of the semiconducting materials typically used in the cells. The four inherent limitations on the efficiency of a single junction photovoltaic cell were first studied and described by Shockley and Quiesser in 1960[12a]. These consist primarily of i) incomplete absorption ii) thermalization iii) thermodynamic loss and iv) radiative recombination.[12b] Incomplete absorption occurs in an inorganic system for any photon that does not have enough energy to bridge the band gap, and in DSSCs when the dye has no absorbance at the wavelength of the incident light in question. It is apparent that an inability to absorb any portion of the incident energy will result in a loss of efficiency as defined in section 1.5.1. Thermalization is the loss of excess energy via thermal relaxation of excited species created by photons with energy that is greater than the band gap. While some driving force is often necessary for electron injection (*cf.* section 1.7.3) any energy above the conduction band of the semiconductor becomes another loss within the system.

Thermodynamic loss pertains to the fact that some energy will always be lost to entropy and other thermodynamic factors such that the energy produced in the external circuit will never be equivalent to the internal energy of the system, which is the difference in energy between the conduction band of the semiconductor and the redox couple in a DSSC. Finally, radiative recombination is the relatively unlikely loss of energy from an excited state through the release of light which allows it to return to the ground state. These inherent limitations and other theoretically removable losses will be discussed in further detail in section 1.5.2.

Methods have been developed to make use of UV light without incurring thermalization losses. In BHJ cells it is possible to have tandem stacks (figure 1.1) that would allow one to essentially absorb the higher energy photons in the first cell and transmit lower energy photons to the second cell where they could be absorbed and used with a lower bandgap anode. To this end there has been considerable research into organic polymers that absorb in the infrared.[24-25] Options for DSSCs that use multiple dyes[26,27] as well as a stacked system similar to the BHJ system[28] have also been investigated but it is difficult to adjust the systems to accommodate the use of near-infrared photons with such low energy. There has also been significant research into methods of using dyes, with particular photoproperties, in DSSCs which allow for the upconversion of infrared light via triplet-triplet annihilation (TTA). This process will be discussed in greater detail in section 1.7.

1.5 Dye sensitized solar cells

DSSCs are the focus of a significant portion of the research that is currently being performed within the realm of photovoltaics. These cells were first reported in 1991[29] and since then there have been significant improvements to the efficiency of the cell as well as gaining a much better understanding of the processes involved in a DSSC and their effect on the working of the cell. A study on the long term stability and efficiency of DSSCs in a non-laboratory environment showed that the DSSCs had a better performance than a Si cell, of similar laboratory rated output, in both the short and long term and that the major factor contributing to degradation of the cell was leaking of solvents.[30] This type of instability related to extrinsic factors was expected[31] and has since been solved by using more advanced cell sealing techniques.[32]

1.5.1 Current efficiencies and limitations

While there are considerations such as cost and ease of production that go into the decision of whether or not a solar cell represents a viable means for electrical energy production, efficiency is the foremost indicator of whether a particular DSSC is worth developing or not. There are many measurements that are used to determine the efficiency of a solar cell but the most common, as well as most standardized, set of measurements are those that determine the power conversion efficiency of a cell. The energy conversion efficiency is simply the measure of energy that is produced by a cell at a given voltage as found on a current vs. voltage graph divided by the total amount of incident energy on the cell. While this seems like a trivial measurement there are many things to consider when actually collecting the data, in particular the nature of the light used to acquire the information necessary for the calculation. Standard photon flux curves, such as figure 1.3, are produced by standards institutions such as American Society for Testing and Materials (ASTM) and Institue of Electrical and Electronics Engineers (IEEE). These curves are used to determine the differences between the illumination produced by a sunlight simulator and that which would actually be available, on a cloudless day, from the sun. Once the differences between the two light sources are ascertained, the spectral sensitivity of the solar cell must be determined by measuring its response at each pertinent wavelength. The two pieces of information are combined into a spectral-mismatch function which will determine how much a given test will over- or under-estimate the efficiency of a solar cell. This correction factor is applied to the measured current vs. voltage curve and the energy produced by the cell is divided by the total energy incident upon the cell, which is the energy per unit area produced by the source multiplied by the active area of the cell exposed to the light, to obtain a conversion efficiency. There are also complications with overestimating efficiencies when the area of the cell is below a threshold value of approximately 1 cm^2 so efficiency measurements are unreliable unless cells are at least that large.[5,33] Needless to say that unless rigorous procedures for the measurement of efficiencies are followed then comparison of cells from different groups is impossible. The difficulty of standardizing measurements between laboratories has led to the practice of having solar cell efficiencies

corroborated by independent testing groups such as NREL if they represent a record breaking efficiency for that type of solar cell.[5]

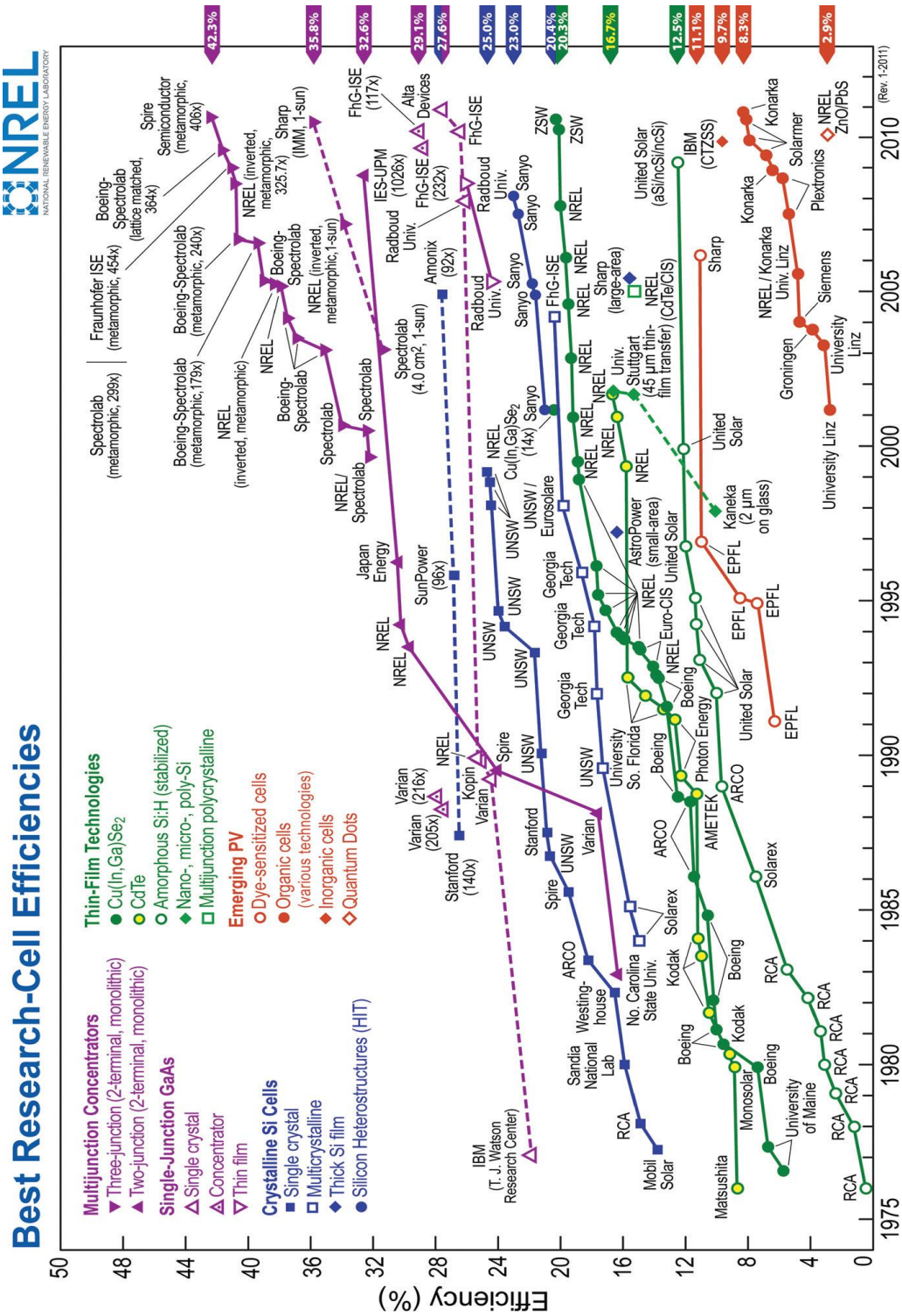

Figure 1.4 History of record breaking efficiencies for different types of solar cells as collected by NREL [4]

Figure 1.4 shows the increasing efficiencies obtained for various types of solar cells. These data indicate significant improvements in the understanding and optimization of photovoltaics but there remain significant hurdles to the commercial implementation of these technologies. Essentially all of the cells discussed in the figure exist only as one-off laboratory creations and because of the time, effort and expertise required to produce a cell of that quality it seems improbable that they will be able to scale up the production of similar cells with the same efficiency. Of course for some of these cells the efficiency is high enough that even if mass-produced cells, based on the model cell, were able to obtain a fraction of the best-cell efficiency they would be valuable. The need to adapt the knowledge gained to a system that can be consistently and relatively easily reproduced becomes the issue and it leads to the search for fundamental transformations of the structure, material and processes involved in solar cell production.

1.5.2 System kinetics and inherent energy losses

In principle, the DSSC presents a relatively straightforward light harvesting system but in reality its operation is greatly complicated by a number of competing processes.

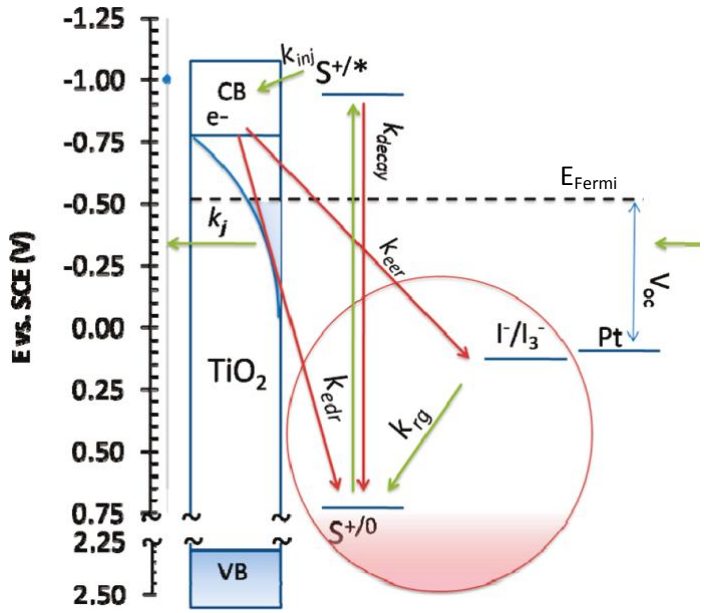

Figure 1.5 Schematic representation of energetic processes in a DSSC. Desirable processes are excitation, electron injection (inj), charge collection (j) and dye regeneration (rg). Undesirable processes are radiative/non-radiative decay (decay), recombination (edr) and interception (eer). Figure adapted from [34]

One method for creating a highly efficient solar energy collection system would be to make the rates of occurrence for favourable processes much faster than the rates of unfavourable processes such that the net contribution of the unfavourable processes to the overall function of the cell is negligible. While this is feasible, cells which take this approach do not appear to be the most efficient cells produced.[35]

The easiest adjustment to make is pushing the system to favour electron injection from the photo-excited state to the semiconducting surface. This can be achieved by either changing the energy level of the excited state or, more simply, adjusting the density of available acceptor states within the conduction band of the semiconductor relative to the dye.[35,36] The density of states in the conduction band of the semiconductor can be lowered simply by adjusting the composition and concentration of the electrolytes within the solution used. By increasing the rate of electron injection the short circuit current (J_{sc}) will, by definition, increase unless the rate of recombination and/or interception are also increasing at the same time. This will not, however, necessarily result in a more efficient cell. As explained in section 1.5.1 the efficiency

of a cell is dependent on both J_{sc} and the open circuit potential (V_{OC}) and V_{OC} is directly affected by the potential of the quasi Fermi level of the semiconductor (see figure 1.5). Figure 1.6 further explains the effect of changes to the Fermi level energy as it relates to the density of states of the excited dye. As the Fermi level drops, relative to the density of states, the rate of electron injection increases as it becomes more energetically favourable. This also explains why increasing the rate of electron injection is not necessarily beneficial to a solar cell's overall efficiency as maximum efficiency can be considered as a minimization of free energy losses. While the empty conduction band states must be low enough in energy that the rate of injection is significantly faster than the rate of decay they must not be so low as to unnecessarily waste energy as thermal loss within the system.

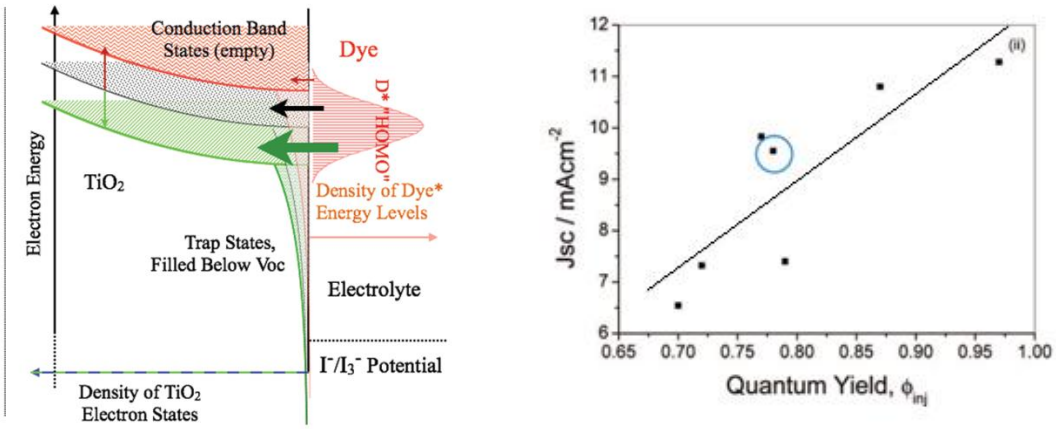

Figure 1.6 (left) representation of three different band edge shifts and the effect on electron injection from the dye.[36] (right) graph of the performance of various cells with differing electrolyte concentrations, most efficient cell is circled in blue.[35]

Once electrons have been injected into the semiconducting surface they begin to diffuse toward the surface of the electrode. At this point the loss of efficiency due to competing processes becomes difficult to generalize. Because many factors that are unique to a particular system can affect the probability of occurrence of processes such as recombination or interception, it will suffice to say that it is necessary to find a system that minimizes these processes.[37-39] At the same time it has been shown that for a system to be efficient it typically needs to have an electron diffusion length, which is equivalent to an average lifetime for

diffusing electrons before they are reabsorbed, that is twice the thickness of the TiO_2 film in the system.[39] It has also been shown that an important (negative) factor to consider when choosing a dye is whether it catalyzes the transfer of electrons from the semiconducting surface to the redox couple.[38]

The last major kinetic process within the cell is the regeneration of the ground state of the dye via the redox couple. It is important that this step be as fast as possible so as to avoid the recombination of a photoinjected electron from the semiconductor with the oxidized species from the redox couple. Fortunately this type of recombination is relatively slow in these systems due to slow electron diffusion through the TiO_2 and the low concentration of electrons compared to the concentration of the reducing agent of the redox couple. However, because of the nature of the redox pair (often I^-/I_3^-) the mechanism for dye regeneration is inherently complex which leads to a rate constant which is several orders of magnitude slower than the diffusion-controlled limit.[34] In order to ensure an acceptable rate of regeneration, most systems are designed to have a regeneration energetic driving force that is greater than or equal to 600mV. A driving force is also maintained between the cathode and the redox pair. While it is important that charge transfer from the cathode to the redox couple also occurs on a fast time scale the loss of energy, which is dissipated as heat and not recaptured, presents a significant barrier to increased efficiency. If a more efficient mechanism for the regeneration of the ground state dye were found a large portion of the energetic losses, as well as potentially destructive heat sources, could be minimized.

1.6 Electron transfer (ET) and electronic energy transfer

There are two main models that pertain to the transfer of electrons within the dye systems used in DSSCs, Rehm-Weller theory and Marcus theory. Both of these models and the two most common energy transfer mechanisms, Dexter and Förster excitation transfer, will be examined in this section.

The Rehm-Weller model was created to predict the Gibbs free energy of photo-induced electron transfer as well as whether a molecule will act as a donor or acceptor, it is based on the following general equation.

$$\Delta G_{ET} = E_{ox}(donor) - E_{red}(acceptor) + C - E^{*} \quad (1.1)$$

In this equation E_{ox} and E_{red} are the standard reduction potentials of the donor and acceptor respectively, C is the Coulomb term and E^{*} is the energy of the photo-excited state.[40a] The Coulomb term is included here to compensate for the fact that the electrochemical potentials are measured in a way that simulates infinite separation from each other when in fact the mechanism requires that they be within a distance that allows for wavefunction overlap if electron transfer is to take place. If they begin as oppositely charged molecules there may be some stabilization of the encounter complex that needs to be formed for transfer to take place which in turn would have a positive effect on the rate of transfer. This model has shown itself to be highly valuable in predicting the correlation between the Gibbs free energy of ET and the rate of fluorescence quenching for a photo-excited species due to electron transfer over a wide variety of energy differences between donors and acceptors.[41] The model predicts that as the Gibbs free energy of the ET process becomes a larger negative number the probability of a transfer taking place, and in turn the rate of ET between the donor and the acceptor, will increase until a maximum rate of transfer is reached. This plateau follows from equation 1.2 where k_q is the rate constant for intermolecular ET, k_d and k_{-d} are the rate constants for the formation and separation, respectively, of the encounter complex, K_d is the ratio of k_d / k_{-d} and Z is the universal collision frequency factor.

$$k_q = \frac{k_d}{1 + \frac{k_d}{K_d Z}\left[\exp\left(\frac{\Delta G^{\ddagger}}{R\,T}\right) + \exp\left(\frac{\Delta G_{ET}}{R\,T}\right)\right]} \quad (1.2)$$

Marcus theory is also a model concerned with electron transfer between a donor and acceptor molecule and, in fact, the two models are often compared. The main difference between the two models is the prediction of an inverted region by Marcus theory where the activation energy of electron transfer begins to increase even though the reaction becomes more energetically favoured.

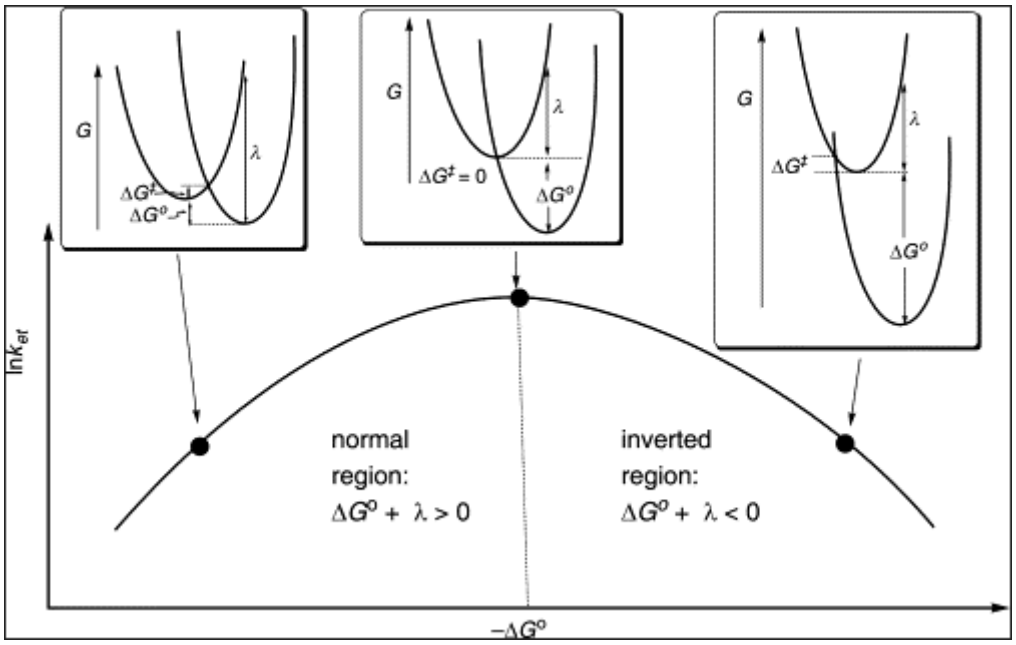

Figure 1.7 Graphical representation of the predicted overlap of potential energy wells in an electron transfer reaction.[40b]

The relationship between the activation energy and the change in free energy can be written as follows;

$$E_a = \Delta G^{\ddagger} = \frac{(\Delta G^{\circ}+\lambda)^2}{4\lambda} \quad (1.3)$$

Here $\Delta G^{\ddagger}$ is the activation energy, ΔG° is the reaction free energy and λ is defined as the reorganization energy, i.e. the energy required to relax to an equilibrium state once electron transfer takes place. The reorganization energy is commonly expressed as the sum of two terms consisting of the energy required for nuclear reorganization of the redox pair and the energy used in reorganization of the solvent environment surrounding the redox pair. Marcus also used his model to predict the exponential decrease in electron transfer as the molecules move farther apart as well as examining the effect that the solvent shells surrounding both the donor and acceptor have on the rate of transfer.[42]

The quadratic dependence of the activation energy on the free energy change leads to a parabolic relationship between k_{ET} and ΔG°, with a maximum at λ = -ΔG° when $\Delta G^{\ddagger} = 0$. This is where the prediction of the inverted region comes from (*cf.* figure 1.7).

The inverted region was not, however, directly observed in photo-excited electron transfer which led to the creation of the Rehm-Weller model, which matched the observed data. Some papers have suggested that Marcus theory is only effective at predicting electrons in dark processes[40a], or in transfers where the change in Gibbs free energy is greater than -15 kcal/mole[41] but recent work by Mataga and coworkers has shown this phenomenon directly in photo-excited charge separation.[43] Mataga proposes that the inverted region was not observed originally in systems with a large change in free energy as the donor and acceptor in these systems were separated by large distances. Since this was the case he observed the photo-excited charge separation from the S_2 state of a Zn porphyrin that had been covalently bound to an imide substituent which allowed for the direct observation and measurement of rates through the normal and the inverted region.

The two most commonly used theoretical models for the transfer of energy between a donor and acceptor are due to Dexter and Förster. The Dexter model involves a short-range energy transfer process that requires orbital overlap between the donor and acceptor. This exchange is related to the models above and the first order rate constant of energy transfer is given by:

$$k_{ET} \propto [h/(2\pi)]\, J \exp[-2r/L] \qquad (1.4)$$

In this equation L is the sum of the van der Waals radii of the donor and acceptor, J is the spectral overlap integral and r is the distance between the centre of the donor and the centre of the acceptor. It is obvious that the distance between the donor and acceptor must be very small as the rate of electron transfer has an exponential dependence on their separation. Similarly, J shows that for this process to take place there also needs to be spectral overlap between the emission and absorption profiles of the donor and acceptor. In Dexter exchange an excited electron from the donor molecule is given to the acceptor molecule while a ground state electron from the acceptor is transferred to the donor (i.e. energy transfer occurs via

electron exchange). This mechanism is the dominant one for energy transfer in TTA and will be further discussed in 1.7.4.

Unlike Dexter energy transfer, Förster energy transfer does not require wavefunction overlap and can take place between donor and acceptor molecules over much greater distances. This is possible because Förster energy transfer makes use of long range dipole-dipole interactions that depend strongly on spectral overlap between the donor emission spectrum and acceptor absorbance spectrum as well as the magnitude and proper orientation of their transition dipoles.

$$k_{EET} = \frac{1}{\tau_D} \left(\frac{R_0}{r}\right)^6 \tag{1.5}$$

This equation is the simplest representation of the model for the rate of electronic energy transfer via the Förster mechanism. τ_D is the lifetime of the donor in the absence of the acceptor, R_0 is the Förster distance which is the distance at which the inverse of the rate of transfer is equal to τ_D, and r is the centre-to-centre distance between the donor and acceptor molecules. In the expanded equation (1.6) it is shown that contained within the R_0 term are two important factors, the spectral overlap function (J) and a parameter which describes the relative orientation of the donor and acceptor in space (κ^2). η and Q_D are the refractive index of the medium and the quantum yield of the donor (in the absence of the acceptor) respectively.

$$k_{EET} = \frac{8.79 \times 10^{-5}\, [\kappa^2 \eta^{-4} Q_D\, J(\lambda)]}{\tau_D\, r^6} \tag{1.6}$$

Both J and κ^2 play a crucial role in the process but in the case of κ^2 it can usually be assumed to be equal to 2/3 for molecules that undergo random rotational diffusion (e.g. in fluid solutions) prior to energy transfer.[44] However, when τ_D << (rate of diffusion)$^{-1}$ this assumption will no longer be valid. This will be the case for porphyrin photophysical processes related to the S_2 state that occur in solution.

1.7 Porphyrin photophysics [45]

While not the most efficient dye system used in DSSCs, porphyrins present a far more robust and more widely tunable dye system than the more efficient Ru-based dye systems such as N719. These dyes are commercially available in a very high purity form and have many desirable properties that can be advantageous in light harvesting systems, including high oscillator strength and very long lived triplet states. For these reasons the work in this thesis has focused on porphyrins and their properties.

1.7.1 Absorption and fluorescence properties

Each porphyrin possesses unique photoproperties that can be adjusted in a variety of ways but 'regular' porphyrins, those which only have π valence electrons, have many similarities. Common synthetic porphyrins exhibit sharp, intense absorption ca. 400-470 nm, corresponding to the B or Soret S_2-S_0 band absorption*, and weaker absorption between 500 and 800 nm attributed to Q band S_1-S_0 transitions (*cf.* figure1.8).[46,47] Most porphyrins show Q bands with both a 0-0 vibronic transition as well as a 1-0 vibronic transition that is more intense as the 0-0 transition cannot take place in a D_{4h} molecule except via symmetry breaking vibrations. There are also less intense transitions further to the UV region of the spectrum which can play a significant role, particularly in fluorescence upconversion.

* It is spectroscopic convention to always list the upper state first. This is done whether a transition is from an upper state to a lower state or not.

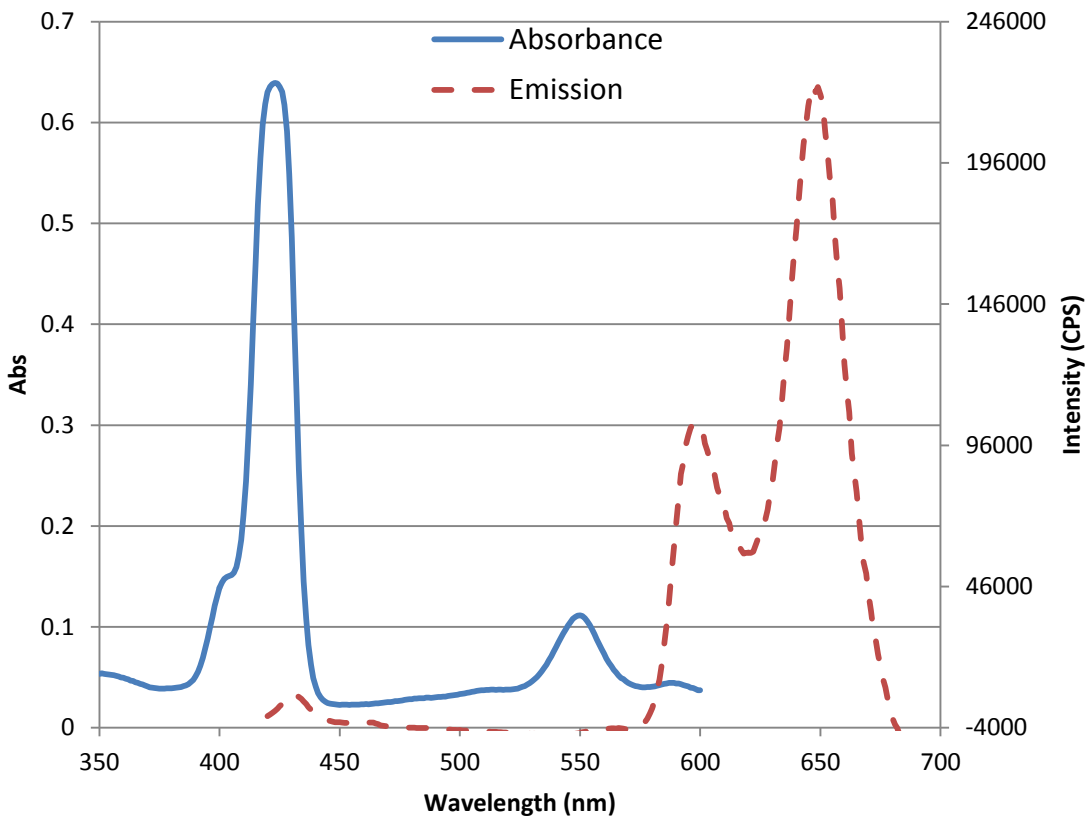

Figure 1.8 Typical absorbance and emission spectra for ZnTPP in toluene

The emission properties of these dyes are not as uniform as the absorption properties but they do show a certain amount of regularity. Although the strongest absorption band (B or Soret) corresponds to an S_0 to S_2 excitation there is usually little to no fluorescence from the S_2 state. The non-radiative decay from S_2 to the S_1 excited state is the favoured relaxation route and the process takes place on a time scale of approximately 10^{-12}-10^{-13} seconds. While almost all porphyrins behave in this manner fluorescence from the S_2 state can occur if the energy gap between the S_2 and S_1 singlet states is large enough (energy gap law), the two excited singlet states' energy surfaces are parallel to each other and, the rates of intersystem crossing to available triplet states located between S_2 and S_1 are slow. The parallel nature of the S_1 and S_2 excited state potential energy surfaces is particularly important as this retards an otherwise rapid non-radiative decay of the S_2 state due to conical intersection of the S_2 and S_1 surfaces.[48] If S_2-S_0 fluorescence occurs it appears as a weak emission band with a maximum at ca. 420-430

nm. The more common radiative decay route, fluorescence from the S_1 state, is also highly dependent on the structure of the molecule and in particular the nature of the central atom. As the central metal becomes heavier it has been shown that the rate of intersystem crossing from the S_1 state to the T_1 state increases which, in turn, lowers the quantum yield of S_1-S_0 fluorescence for the molecule. This increase in the population of the triplet state will generally increase the quantum yield of phosphorescence as well but the heavy atom effect can also increase the rate of non-radiative decay from T_1 to S_0 in much the same way as it does from S_1 to T_1 thus negating the increased rate of population of the triplet state. Phosphorescence, if visible, shows weak emission in the far red to near infrared region of the spectrum (ca. 750 nm). It is possible for heavy atoms on external substituents (particularly halogens) and counterions coordinated to the central metal to create a similar heavy atom effect.[49]

1.7.2 Tuning dye photoproperties

While it is possible to adjust the photoproperties of any molecular system through synthetic or environmental changes, the chemistry involved in producing significant changes can often be extremely difficult. The depth of study that has gone into synthetic manipulation of porphyrins, as well as the effects of such manipulations, provides a strong foundation for the development of optimized porphyrin dye systems.[46,50] However, the formation of a porphyrin dye system that both absorbs strongly across the solar spectrum and has good energy transfer efficiency within the cell still poses a difficult problem and there have been many different approaches taken to the creation of such a system.

Manipulation of the ligands surrounding the porphyrin ring is one of the most common approaches to photoproperty design. It is relatively easy to selectively react one or more of the twelve functionalization sites on the macrocycle ring and there are a number of synthetic procedures that have been developed for doing this in a clean facile way. These procedures often take advantage of metal catalyzed procedures, such as Sonogashira cross-coupling[51] or Huisgen cycloaddition[52], which are highly efficient and result in clean products that need minimal purification. This in turn allows for the synthesis of an extremely wide range of

porphyrin dyes that can be used in many different applications. Figure 1.9 shows the effects that even relatively small changes to the ligands surrounding the porphyrin ring can have.

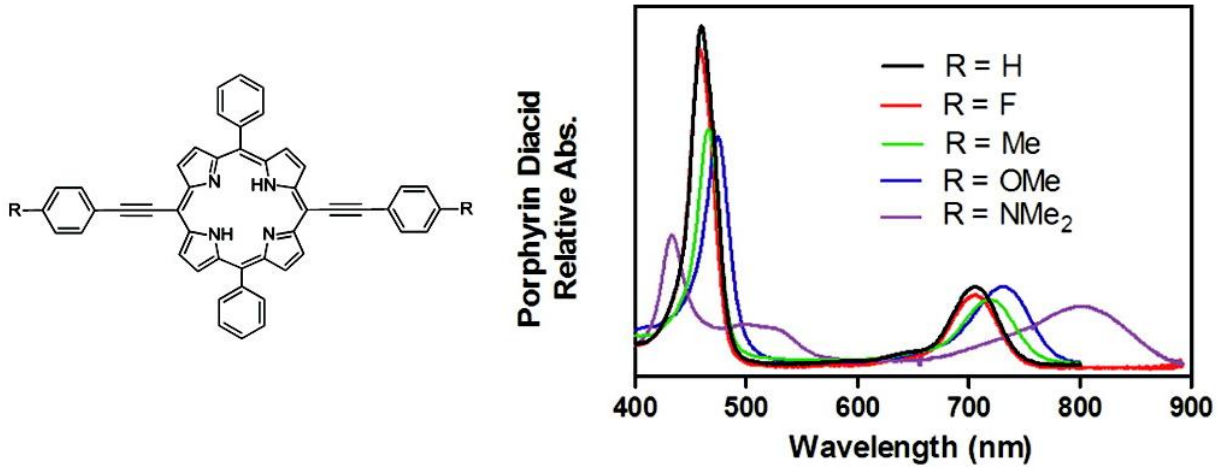

Figure 1.9 Ligand effects on dye absorption properties, measured in toluene.[46]

These ligand effects are most pronounced when the conjugation of the dye system is altered or extended. For this reason highly conjugated ligands oriented in the same plane as the porphyrin ring are often used if dramatic changes are needed. This can be accomplished in two ways; i) the attachment of planar aromatic ligands, at the β position, that do not have steric interference with the porphyrin ring or ii) directly bonding aromatic rings to the pyrrole subunits (e.g. naphthalene fused porphyrins[53] or phthalocyanines[54]). This extension of the conjugation system generally results in a red shift and broadening of the porphyrin absorption bands as well as an increase in oscillator strength in the Q bands.[46,55] Knowing that the absorption profile of the dye can be red shifted and broadened, which are both useful for increasing solar cell efficiency, it would seem logical to simply make very large π-conjugated systems and tether them to the surface of the semiconductor. As is often the case though, secondary effects need to be considered. Large conjugated systems tend to π stack with each other causing large amounts of aggregation within the system. Uncontrolled aggregation greatly increases the number of available non-radiative decay pathways of photoexcited electronic states, which can have a significant impact on efficiency.

Linking molecules to the metal centre of a porphyrin is another common route for photoproperty manipulation. This can include self-assembled non-covalent complexation as well as covalent linkage between the metal and any other molecule. These types of linkages can be used to form supramolecular structures or to simply affect the properties of the porphyrin monomers that are ligated.[56] For the purposes of this work it is typically considered counterproductive to ligate individual monomers as this will sterically hinder individual dyes from approaching each other which can in turn retard TTA[57](*cf.* Section 1.7.4). However, the ligation of a porphyrin to form supramolecular structures has the potential to increase the rate of TTA because tethering the individual dyes at a distance that favours interactions between dyes that have been excited will increase the probability that triplets will undergo annihilation before they decay. For these reasons the choice of solvent for a system must also be made with the effects of central metal atom ligation in mind as a coordinating solvent will essentially act as a linker[57] that blocks the wavefunction overlap needed for TTA. The dependence of the efficiency of TTA on distance between interacting triplets and the actual model for these interactions will be further discussed in section 1.7.4.

1.7.3 Excited state lifetimes and electron injection kinetics

The kinetics of electron transfer from the excited states of the dye to an acceptor will be a primary determinant in the ability of the cell to efficiently collect and utilize solar energy. The ability to produce an excited state that is sufficiently long-lived to transfer an electron to the semiconductor is crucial in DSSCs. In systems where the excited state of the dye is energetically higher than the conduction band of the semiconductor, electron injection has been shown to occur at rates faster than 1 ps[37] but, while this is relatively fast, highly excited states, such as S_2 in the porphyrins, also tend to have very short lifetimes. For this reason, it is much more useful to use porphyrins whose central metal atom has a completely full or completely empty d orbital as their excited states tend to be much longer lived.[58] One of the most commonly studied closed d shell porphyrins is zinc tetraphenylporphyrin (ZnTPP) whose S_2 lifetime in solution ranges from approximately 240 fs to 3.5 ps depending on the solvent.[59,60] Other dyes that are more commonly used in DSSCs tend to have longer lived excited states, most notably N719

appears to inject electrons from an excited triplet state which has a lifetime on the order of 6 ns[61] which would greatly increase the probability of electron injection. However, current studies have shown that the most efficient systems are not necessarily those with the fastest injection kinetics and longest lived excited states but those whose electron injection rate is just fast enough to compete with the rate of competing radiationless decay from the excited state to the ground state.[62]

The process of electron injection from an excited chromophore to an attached semiconductor is complex and can take a number of different routes. Regardless of the electron transfer (ET) mechanism used there are a number of general factors that influence the process and the rate at which it occurs. As discussed above, the availability of acceptor states within the semiconductor and the energy of the excited dye play significant roles in the process and these can often be tuned to produce optimized conditions. Another factor is the amount of orbital overlap present between the LUMO of the dye (occupied upon photoexcitation) and the acceptor conduction band (CB) of the semiconductor. In systems with significant overlap, models have predicted that electrons from the dye delocalize onto the semiconductor surface and ET can take place at a rate as fast as 10 fs. This type of strong coupling tends to favour an adiabatic ET mechanism which allows for electron transfer near the CB edge, which will also minimize voltage losses that occur with injection into semiconductor hot bands. It is possible to still have efficient ET in systems that don't have this strong coupling but ET will proceed through a non-adiabatic mechanism that depends on a large number of available acceptor states resulting in a loss of open circuit potential. However, this loss is potentially offset by a decrease in recombination losses once ET has taken place, resulting in a larger overall current. The advantages and disadvantages of these different processes allows for many different routes to be taken towards the optimization of a cell.[37,63]

The coupling of a system can be impacted significantly by the method which is used to link it to the semiconductor. Most studies suggest that electrons are more likely to travel via bridging molecules rather than through the space separating the dye from the surface, which means that the position and nature of the bridging group is very important when considering coupling

effects. Carboxylate anchoring groups, for example, tend to favour electron injection as they allow delocalization of the LUMO orbital of the dye toward the surface. The delocalization of the electron density toward the semiconductor is ideal, which is why axial out-of-plane bridging molecules appear to be less useful for porphyrin systems than peripheral anchoring groups which extend the conjugation.[64]

Another problem facing porphyrin-based DSSCs is the tendency for porphyrins to form aggregates due to π stacking affects and their general lack of solubility in organic solvents.[37,64] These aggregates often decrease lifetimes of excited states even further by providing more non-radiative relaxation pathways for the dissipation of energy within the photoexcited molecule(s). This makes it necessary either to block the formation of aggregates using coadsorbed acids or bulky peripheral ligands, or to promote the formation of regular aggregates that have more desirable properties.

1.7.4 Triplet triplet annihilation

Photon upconversion is a very promising avenue of research in the effort to increase the viability of solar energy harvesting. Photon upconversion involves combining the energy absorbed from two low energy photons to generate a higher energy species. By increasing the spectral range of solar photons that can be used by the system to produce energy, upconversion allows for otherwise unattainable photovoltaic cell efficiencies. The most common method of upconversion in dye systems that are useful in DSSCs is TTA.

TTA involves the transfer of energy from a donor molecule in an excited triplet state to a second molecule also in a triplet state, resulting in a more highly excited acceptor molecule in a singlet state and a ground singlet state donor molecule. This process makes use of molecules in the triplet state as their relatively long lifetimes, on the order of μs to ms, allow them to maintain their energy long enough for diffusion limited processes to take place. When choosing TTA systems it is also important to consider the relative energies of their various excited states. The excited singlet state that needs to be attained can be no more than twice the energy of the triplet state or it will not be possible to combine the energies from two triplet excited states and gain enough energy to populate the excited singlet state product.[65] Figure 1.10 shows an

example of triplet triplet annihilation where the absorbers also act as the upconverters. In this system two separate molecules absorb a photon and are each excited to the first singlet state which then decays to the first triplet state. Once these molecules encounter each other it is possible for one of them to donate their triplet energy to the other thus promoting it to the excited singlet state. In porphyrin systems ($2\ T_1 \rightarrow S_2 + S_0$) is energetically possible which means that porphyrins can act as both the absorber and the upconverter. This type of homomolecular TTA is very common in the metallated porphyrin systems that are of particular interest to this work.

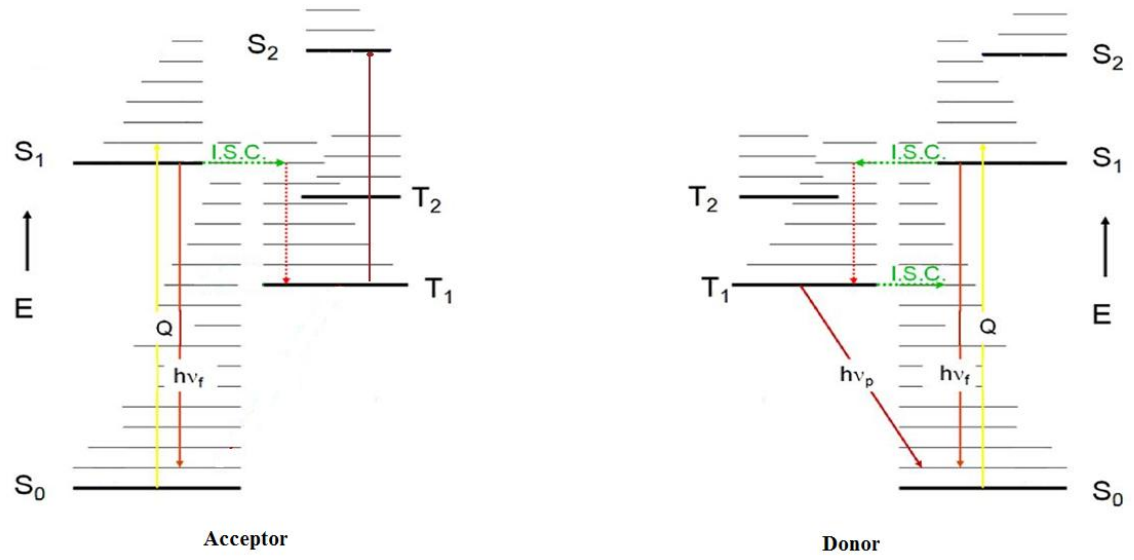

Figure 1.10 Jablonski diagram of the energetics of a porphyrin homomolecular TTA system

There are a variety of mechanisms which can lead to TTA. One route includes absorption of a photon by a donor molecule which, following intersystem crossing (ISC) from a singlet state to triplet state, donates energy by triplet-triplet energy transfer to an acceptor molecule which can then undergo TTA when it encounters another acceptor in the triplet state. A second route is when a system contains two different molecules in triplet states. In these heteromolecular systems one or both of the molecules may act as both the absorber molecule and the triplet molecule that undergoes TTA. Often the systems which are capable of using molecules that both absorb and upconvert are more efficient as there is less complexity in the overall

mechanism as well as shorter times between viable encounters. The last case, homomolecular TTA, is the simplest TTA mechanism and the process of foremost interest in this work as it applies to TTA in porphyrins. In this type of homomolecular TTA the porphyrin is used as both the absorber and the upconverter since twice the energy of the first excited triplet state is slightly greater than the energy of the second singlet state in most closed shell metallated porphyrins.

The primary requirements for efficient TTA that can increase DSSC performance are a long-lived triplet, strong absorbance in the red and near infrared (NIR) portions of the solar spectrum and the ability to approach another excited molecule relatively closely. A long-lived triplet is necessary as the process of TTA in solution is diffusion limited and the rate of successful encounters between two triplets can be relatively slow depending on solvent properties, the concentration of dye present in the solution, the absorbed intensity and whether or not the dyes are confined to a particular volume. Similar properties are important in solid state TTA where exciton migration and interaction is the mechanism for TTA instead of encounters between molecular triplet states. Absorbance in the red/NIR is important as the whole purpose of TTA is to allow the cell to take advantage of the large number of low energy incident photons present in natural sunlight. The ability of the triplet dye molecules (or excitons) to interact with each other is crucial to the efficiency of the TTA process.

Porphyrin dye systems that are used in DSSCs generally consist of a number of solvated dyes that are either permanently linked to a semiconducor nanoparticle or are at least able to form a transient bond with the semiconductor (*cf.* section 1.7.3). The process of TTA in these systems follows the scheme ($2\ T_1 \longrightarrow S_2 + S_0$) which makes the steady-state concentration of triplets in solution one of the primary limiting factors of the overall process. In closed shell porphyrin systems nearly all molecules end up in the S_1 excited state upon absorption of a photon whether they are excited directly to the S_1 state or to a higher singlet state. The high internal conversion efficiency from S_2 to S_1 and the large S_1 to T_1 ISC yield (the quantum yield of fluorescence from the S_1 state of these molecules is typically low[66]) allows for the creation of many triplets. Once triplets are generated and encounter one another they can then undergo

TTA. As mentioned above (section 1.6) the Dexter energy transfer mechanism, which is the model that applies to TTA, requires that the triplet excited dye molecules approach each other closely for energy transfer to take place. Functionally the key orbitals of the molecules have to approach within approximately 5 angstroms of each other for TTA to take place which can lead to problems when the dyes have bulky peripheral ligands or axial ligands that tend to keep the porphyrin rings apart.[57,67]

1.8 Energy gap law

One of the most fundamental laws governing energy transfer is the energy gap law (EGL). The EGL simply states that the probability of radiationless intramolecular energy transfer between two weakly coupled electronic states is inversely proportional to the exponential of the electronic energy gap (ΔE) between the two states. In other words the first order rate constant for radiationless decay decreases exponentially as the energy gap between the two coupled states increases. This explains why the higher excited states (S_n n>1) in most polyatomic molecules display little or no fluorescence as the electronic states higher than S_1 tend to be closely spaced. The S_1 state on the other hand has a relatively large energy gap between itself and the ground state. For this reason the radiationless decay from S_1 is much slower than from S_n (n>1) allowing S_1 fluorescence to take place before its population is depleted. The EGL applies not only to internal conversion between states of the same electron spin multiplicity but also to intersystem crossing between states of different electron spin multiplicity which means that the closer in energy the S_1 state of a polyatomic molecule is to the T_1 state the faster the rate of population of the triplet becomes.[44,68]

The second major consideration for rates of energy transfer is the Franck-Condon factor (FC). The FC is the square integral of the overlap between vibrational wavefunctions of the initial and final electronic states involved in the transition. Since a greater amount of overlap between the two states makes a transition more likely to take place, a larger FC means a faster rate of non-radiative energy transfer. The rate of non-radiative decay (k_{nr}) is related to this factor by the following equation:

$$k_{nr} \propto V^2 F \qquad (1.7)$$

where V is the intramolecular electronic coupling energy and F is the density-of-vibrational-states weighted Franck-Condon factor. Because this value is related to the density-of-vibrational-states, as the energy gap between the inital and final electronic states (ΔE) increases and the overlap of the states decreases, exponentially, we see an exponential decrease in F. This is where the exponential dependence on the energy gap for non-radiative transitions comes from.[44,68] Therefore, when a graph of the natural log of the rate of relaxation via non-radiative pathways versus ΔE is plotted a linear relationship should be evident.

However, this inverse exponential dependence of non-radiative transfer rates on ΔE is only apparent in cases where the intramolecular electronic coupling energy (V) is relatively small, i.e. the weak coupling limit. The weak coupling limit, which is typical of internal conversion and intersystem crossing in aromatic hydrocarbons, is the case where

$$E_M \approx \hbar\langle\omega\rangle \tag{1.8}$$

where E_M is the molecular rearrangement energy and $\langle\omega\rangle$ is the mean vibrational frequency of the state. This means that a relatively small displacement in the normal vibrational modes will take place from one electronic state to the next resulting in F having a much greater influence on k_{nr} than V^2 in equation 1.7. In cases where the weak coupling limit holds the energy gap law holds as well. The opposite case is the strong coupling limit where

$$E_M \gg \hbar\langle\omega\rangle \tag{1.9}$$

which will lead to a large relative displacement of the energy surfaces between the initial and final electronic states involved in the transition. Transitions that fall under the strong coupling limit will not adhere to the energy gap law but will instead have a strong dependence on the activation energy required for transition and in turn the mean vibrational frequency of the molecule will strongly determine whether a transition occurs or not.[69]

1.9 Supramolecular porphyrin studies

There have been a number of groups that have studied a variety of methods for linking porphyrins into supramolecular structures that exhibit novel properties. While many of the

resulting products[70,71] are of little concern to this project some of them are closely related to the types of porphyrin stacks that this study is interested in for use in DSSCs. It has been shown that porphyrins can be bound cofacially in a number of different ways, typically this is accomplished using a meso bridging molecule that forms the porphyrins into a 'tweezer' type molecule[72] but it has been clearly shown that porphyrin dimers linked via their central metal atom will form under the proper circumstances.[73] Furthermore, past work by the Sanders group[74] has provided a foundation for predicting the behaviour of porphyrin dimers which allows for a more logical planning process when approaching the synthesis of a supramolecular construct that must fill a certain role within a system.

1.10 Objectives

This work will endeavour to look into the viability of DSSCs in general and it will specifically apply the background information provided in this section to two unique dye systems that show potential for use in an efficient photovoltaic cell. ZnTPP and tin(IV)-dichloro tetraphenylporphyrin ($SnCl_2TPP$) are closed D shell metalloporphyrins which possess photophysical properties which make them ideal for the TTA experimentation undertaken in this project. Their long lived triplet states and ability to either approach other molecules closely or be linked to other dye molecules directly allows them to act as efficient homomolecular systems (*cf.* section 1.7.4). Different modifications of these dye systems will be tested and methods for the production of unique supramolecular structures will be described.

By measuring and interpreting the response of the dye systems in varied environments it should prove possible to determine whether they will be as well suited for DSSC work as was anticipated based on the known properties of the individual dye molecules. Whether or not these particular dyes prove to be ideal for a DSSC the systematic measurement of their relevant properties will likely allow for a more structured approach to dye selection in the future.

The thesis is divided into five chapters. The present chapter serves as the introduction to the topic and provides the background information necessary to gain a working knowledge of the project. The specific information related to the experimental parameters is detailed in chapter two and the results of those experiments are collected in the third chapter. Chapter four

contains a discussion of the results and the fifth chapter contains a summary of the project to date as well as recommendations for future work.

2. Experimental

2.1 General methods and materials:

All chemicals were used as received from the designated supplier, unless otherwise specified. Experiments were performed at room temperature in aerated solution unless specified that they were purged. When samples were purged, ultra pure argon or nitrogen gas was passed through the solution for 15 minutes prior to the measurement and an overpressure of inert gas was maintained within the cell if possible.

2.2 Electronic absorption spectra

Absorbance data have been used to measure changes to the electronic spectrum of a compound caused by manipulation of its molecular structure. Typically, in the experiments reported in this thesis, a significant change in the electronic structure comes about from changes to the symmetry of a molecule or a change in the extent of conjugation within the molecule. For this reason absorption spectra were used for confirmation of structural changes following synthetic procedures. Along with this information absorption measurements also provided the information necessary to perform other experiments by giving values for the energy required to excite the compounds to the desired state for observation.

2.2.1 Instrument properties

A Varian Cary 500 spectrophotometer was used for all absorbance measurements. The spectrophotometer was typically scanned over a range from 300 nm to 750 nm at a rate of 10 nm/second with an integration time of 0.1 seconds and a slit width of 1.0 mm. The linear spectral dispersion of the spectrophotometer at these settings is approximately 1.0 nm/mm which gives a spectral bandwidth of 1 nm. By using the double beam mode it was possible to place a matched cuvette with the solvent and any other non-dye components of the solution in the reference compartment and thereby measure only the changes to the porphyrins within the system. When using special cells (i.e. spectroelectrochemical cells), a matched cell was unavailable so the reference beam was simply passed through air. To compensate, a blank scan

was taken with the cell empty and the resulting spectrum was subtracted from all other data obtained during the experiment to create background corrected spectra.

2.2.2. Data treatment

Data was converted from the DSW file type collected using the Varian software to an ASCII format and imported into a spreadsheet for analysis. The spectra that were obtained from the electronic absorption data measurements were normalized for instrument baseline drift and compared directly. This was accomplished by first identifying a flat portion of the spectrum common to each scan and normalizing the point to a common value. Once spectra were plotted and normalized within a spreadsheet program, the peak picker function was used to assign the wavelength of the maximum point on a peak. Once these points were identified, differences between spectra were examined and quantified. Peak shifts as well as changes in peak intensity were used to analyze the changes that take place within the system being studied.

2.3 Emission spectra

One of the primary means of monitoring changes to the dye systems used in this project were measurements of emission spectra which have the ability to detect changes to very small portions of the total dye population being studied as long as the quantum yield of fluorescence is reasonable. By measuring the fluorescence of the dye at particular excitation wavelengths it was possible to observe many things directly, such as the ability of the dye to upconvert light or the quenching properties that the system exhibited. The titration of a porphyrin system with a ligand capable of linking to the metal centre was observed using emission spectroscopy as well as monitoring the polymerization of porphyrins into antenna-type stacks. It is particularly useful that these measurements can be done with very small amounts of the dye being studied (μM concentration) and the sample is typically not destroyed by the process as long as it is relatively photostable.

2.3.1 Instrument schematics and properties

A Photon Technology International (PTI) QuantaMaster fluorometer was used for the collection of emission spectra including a 75 watt xenon arc lamp which was used as the excitation source for all standard fluorescence measurements. The light from this source was passed through a double monochromator and adjustable slits before hitting the sample. The original sample holder set up was made to accommodate a standard (12.5 x 12.5 mm) quartz cuvette with a 10 mm optical path length which was used for all solution phase measurements. The fluorescence emitted by the sample was collected by a lens and passed through another double monochromator and slit combination before being detected by a PTI model R928 photomultiplier tube (PMT). When higher power was needed for excitation it was possible to bypass the xenon lamp and excitation monochromators and excite the sample directly with an external source, such as a laser. The detection of the system fluorescence was accomplished in the same way as when the xenon arc lamp was used to excite the sample although the use of a notch filter chosen for the excitation wavelength was often necessary to keep reflected excitation light from masking the signal or damaging the detector. To reduce the noise from scattered excitation light within the sample compartment it was helpful to have a beam dump or other means for collecting excitation light that is directly reflected from the sample. The properties of the system allow for excitation over a range from 240 nm to 1200 nm when using the xenon lamp and emission detection over a range from approximately 180 nm to 900 nm using the R928 PMT and 900 nm to 2200 nm when using the thermo-electronically cooled InGaAs near infrared detector.

2.3.2 Data treatment

Data were plotted directly using the PTI software during collection and exported to a spreadsheet program for further analysis. The spectra were automatically corrected for the sensitivity of the detector by applying a factory-supplied correction factor to the collected data. It was also necessary to correct for the intensity of the xenon arc lamp when performing excitation scans. This was accomplished using a beam splitter in the excitation path to send a small portion of the excitation beam to a calibrated photodiode before it reached the sample.

The software automatically applied the necessary corrections to the spectra based on the measured intensity of the lamp. Spectra were normalized within the spreadsheet as described in the data treatment portion of the electronic absorption spectra section above. Additionally, emission spectra were corrected for reabsorption (inner filter effects) using the formula $I_{corr}=I_{expt}10^{0.44(Aex+Aem)}$ where I_{expt} is the experimental intensity of the fluorescence and A_{ex} and A_{em} are the absorbance of the sample at the excitation wavelength and emission wavelength respectively. The value of 0.44 is an experimentally determined value related to the light path from the point where excitation occurs to the point at the interior of the cell where fluorescence originates.[75,76]

By plotting the graphs in one window it was possible to directly observe changes to peak intensities as well as measure the area under individual peaks within the spectra. The peak picker function and integration tools within the spreadsheet were used to accomplish this.

2.4 Time correlated single photon counting

The lifetime of the excited states of the dyes used in the experiments reported in this thesis are directly related to many of the properties of the solar cells they are associated with. The measurement of the lifetimes of relatively short-lived states allows for the selection of ideal chemical systems as well as the optimization of systems to reduce losses due to transfer of energy from excited states to pathways other than the desired one. Again these measurements were done with very little sample and relatively high sensitivity but it was necessary for the sample to have relatively good absorbance within the stable lasing range of the excitation system, including the second or third harmonic when sufficient power is available, as well as having a reasonable quantum yield of fluorescence.

2.4.1 Alignment procedures, instrument schematics and properties

A Coherent Verdi 10 Watt 532 nm Nd:YAG laser is used to pump a Coherent Mira 900 femtosecond pulsed tuneable wavelength Ti:Sapphire laser which, along with the pulse picker (Coherent model 9200), is used to excite the samples. This setup, together with the second harmonic generator (SHG) and third harmonic generator (THG) crystals, is capable of exciting

samples over a wide range of wavelengths. The laser itself can be consistently used over a range spanning from approximately 700 nm to 1000 nm and using the SHG and THG crystals a range from approximately 240 nm to 500 nm is also accessible. When using the SHG crystal approximately 10% of the incident light was converted to the frequency doubled wavelength and when using THG crystals this value dropped to approximately 1%. A beam splitter placed after the pulse picker sends part of the beam to a photodiode which in turn sends a start signal through a delay line and to a data acquisition board. This signal gives a time reference for the delay between the excitation of the sample and fluorescence collected through the monochromator and detected by the water cooled Hamamatsu R3809U-51 photomultiplier tube. A profile of the lifetime(s) of an excited state can be obtained by measuring the number of photons detected from the sample at different times after each excitation pulse. The range of reliably measurable lifetimes for this instrument runs from approximately 200 picoseconds to 100 nanoseconds. Once the laser light had passed through the beam splitter it was reflected by a series of optimized optics, passed through any necessary harmonic generating crystals and then exited the laser housing. Once outside the laser housing the beam was aligned using a set of high efficiency mirrors mounted on an optical table such that it passed into the sample collection chamber and through a standard cuvette (typically a 2 x 10 mm path length was used) containing the sample. After excitation of the sample the beam exited the sample compartment and terminated in a beam dump.

2.4.2 Data acquisition

Fluorescence from the sample was passed through a magic angle polarizer, collected by another lens and sent to the detector. A magic angle polarizer is used to cancel out any artifacts introduced to the decay profile due to molecular reorientation effects. By polarizing the fluorescence at this particular angle there is essentially an equal chance of a molecule rotating into the plane of fluorescence as it has of rotating out of plane which will produce a null net effect on the decay profile[77]. If the emitted light from the sample was close to the excitation wavelength, a band pass filter was used to block scattered excitation light and avoid detector saturation. Data was collected using a Becker-Hikl SPC 830 data acquisition board and the

accompanying SPCM software module (version 9.30). Each photon detected was sorted into a bin based on the time lapse from excitation to detection. Each bin represents a different time delay that was adjusted to suit the experiment by changing the number of bins or the overall timescale that the bins span within the setup section of the SPCM software. Once this data had been acquired it was necessary to measure the instrument response function (IRF) for the system so that we could deconvolute the signal that was obtained. To do this it was necessary to use a light scattering sample, consisting of a suspension of Ludox in distilled water, and observe photons at the excitation wavelength. The data was then used during the analysis portion of the experiment.

2.4.3 Data treatment

Once the data had been collected using the SPCM software it was exported as an ASCII file by opening the data, selecting 2D trace parameters and then selecting export trace data. The ASCII data was then analyzed using the PSDecay2000 program developed in-house by A. Warsylewicz. By inputting the decay data along with the IRF the lifetime of the decay was analyzed by fitting an iterative convolution of a set of trial decay functions, that have the general formula $I(t)=\Sigma a_i \exp\{-t/\tau_i\}$, with the IRF until a minimum value of the least squares residuals is obtained. Least squares curve fitting experimentally determines the line that has the best fit to the experimental data by varying set parameters (a_i and τ_i) within the function until the desired minimum value is obtained. This residual is the difference between the data point proposed by the equation obtained through iterative convolutions and the experimentally obtained data point. It was necessary to have some idea of the number of decays expected for a particular sample as well as a fair approximation of how long those decays might be to achieve efficient analysis of the data but it was possible to do the analysis through trial and error if this information was not available. To determine whether the fit was acceptable or not there were a number of statistical measures built into the analysis software. The χ^2 value is the measure of the sum of the residual squares and the Durbin-Watson (DW) parameter gives information on serial correlation within the linear regression analysis. Serial correlation occurs when there is a relationship between data points based on the time separation between those two points, this

occurs when there are underlying time dependent functions affecting the data. Typically a fit with a χ^2 value of 1.00 ± 0.20 and a DW value greater than 1.7 (single exponential), 1.75 (biexponential) or 1.8 (triexponential) indicates a good fit. The fit should be attempted with as few exponentials as possible as fitting with more exponentials than actually exist can result in artificially good statistical fits.

2.5 Spectroelectrochemistry

In an effort to create a system with the optimal TTA arrangement it may be necessary to force the aggregation of dyes. A simple and straightforward way to form aggregates that are useful for solar cell applications is the electrochemical synthesis of stacked porphyrins. By tethering metalloporphyrins together at a relatively close distance through axial bonds to the metal, the probability of two porphyrins in the triplet state encountering each other and undergoing TTA may be significantly increased. To determine qualitatively whether or not an electrochemical synthesis had taken place, it was useful to monitor various spectroscopic properties such as the absorbance and fluorescence of the compound in-situ. A cell was therefore devised where spectroscopic data could be measured while the electrochemical synthesis of an aggregated porphyrin structure was taking place.

2.5.1 Cell design

When designing the cell, it became apparent that the best setup for acquisition of the desired information would be a small volume cell with a large electrode surface area. This made it possible to exhaustively reduce the molecules within the cell in a short amount of time, giving a much higher signal to noise ratio when looking at the spectroscopic properties of the aggregated porphyrins. To this end a first generation cell was created where a quartz window and an ITO working electrode were used to give an optical path through the cell while not compromising the electrochemical functionality.

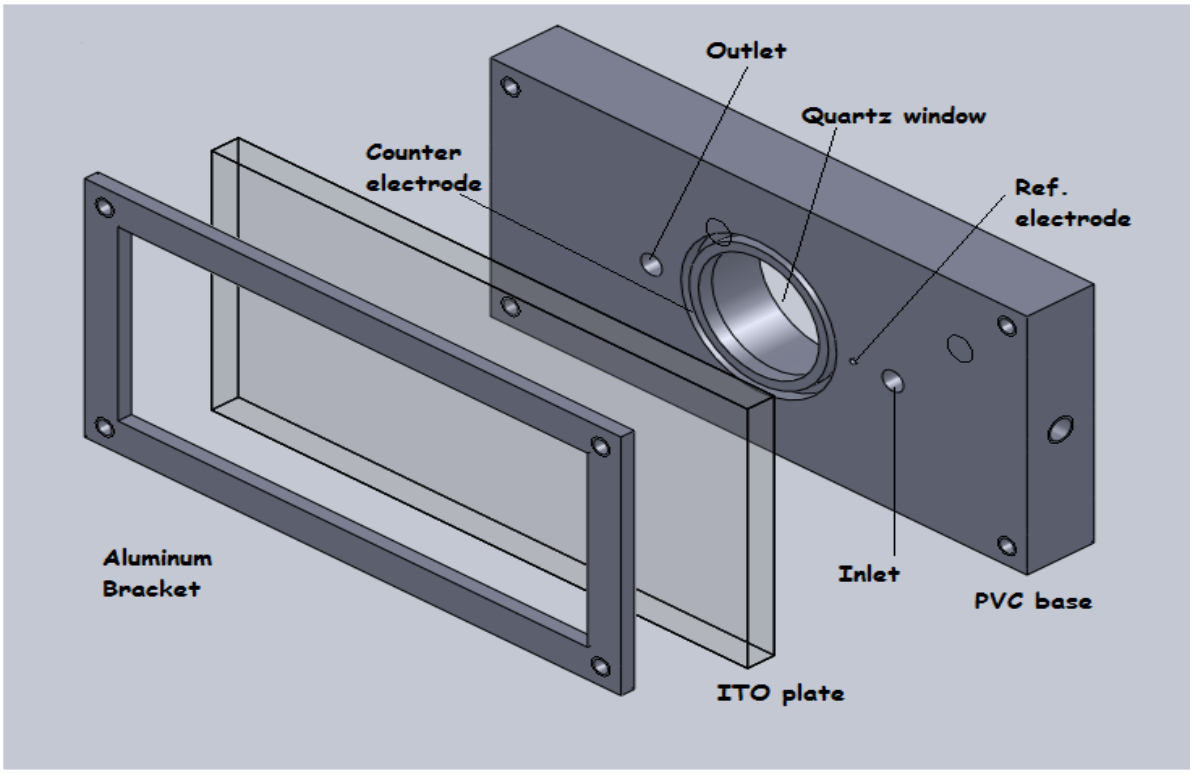

Figure 2.1: Spectroelectrochemical cell made from PVC. A silver wire pseudo reference electrode and gold wire counter electrode were used for our experiments. Not shown in the diagram is the gasket which was sandwiched between the ITO plate and PVC base to provide room for the sample.

However, due to the relatively small number of solvents that $SnCl_2TPP$ is soluble in and the effects of those on the original PVC cell it became necessary to look at another option for these measurements. A second cell was designed (Figure 2.2) where two ITO plates were sandwiched together spaced only by a gasket. These plates were used as the working and counter electrode and a silver wire was once more used as a pseudo reference electrode. Degassed solution was passed in and out of the cell via an inlet and outlet that were attached to tubing containing a Teflon stopcock to prevent the oxygenation of the sample and mass transport between the cell and the exterior once the experiment had begun. The plates were held tightly using clamps to prevent solution leaking from the system.

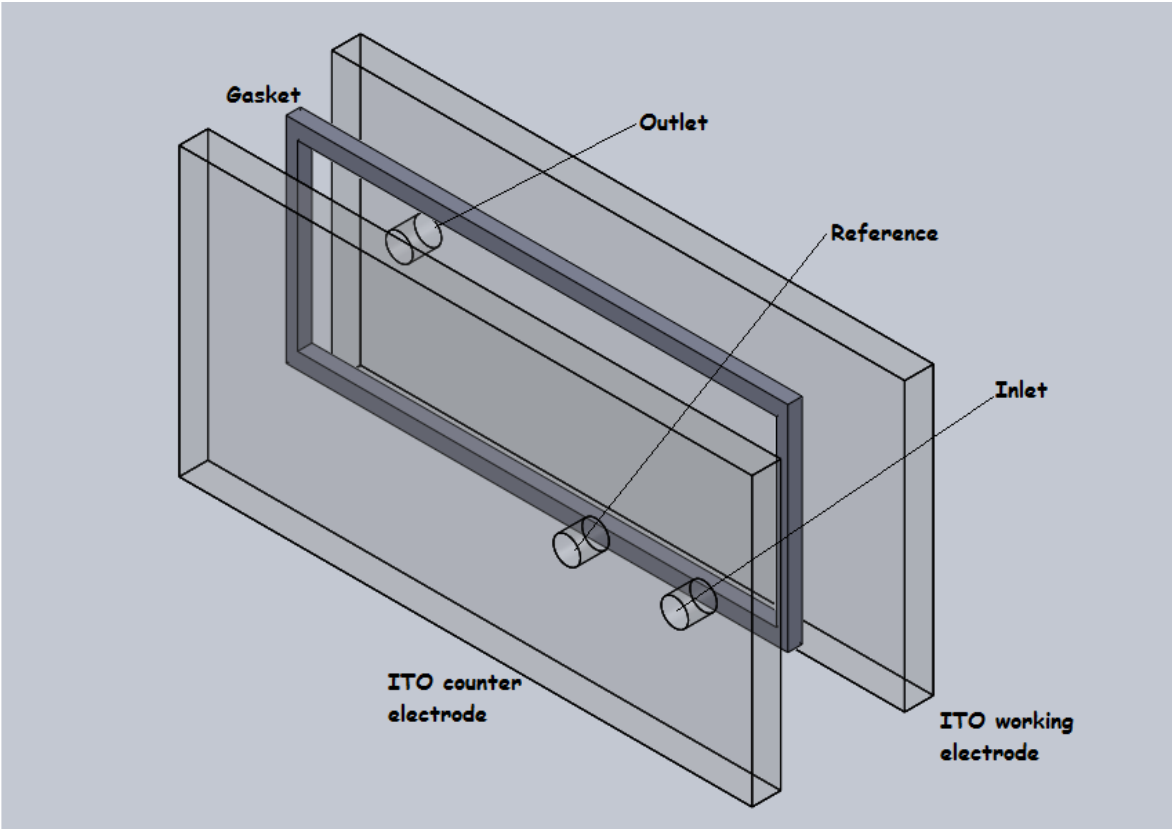

Figure 2.2: ITO spectroelectrochemical cell. Rubber tubing attached to a stopcock was connected to both the inlet and outlet holes via plastic fittings that were epoxied to the non-conductive side of the ITO plate.

When using the ITO cell it was important that some separation be maintained between the two plates to avoid shorting the circuit between the working and counter electrode.

2.5.2 Data acquisition

A mixture of tetrabutylammonium hexaafluoroborate (50.0 mM), benzoquinone (0.6 mM) and $SnCl_2TPP$ (30.0 μM), dissolved in acetonitrile, was used for these experiments. It was important that the acetonitrile be freshly distilled as it has a tendency to absorb water which would significantly limit the available electrochemical window by introducing a significant source of hydrogen evolution. The synthetic goal was to bind the tin porphyrins together using the doubly reduced benzoquinone as a linker between the metal centres. The tetrabutylammonium-tetrafluoroborate acted as the electrolyte for the reaction.

While performing this experiment it was necessary to adjust the sample holders for fluorescence and absorption measurements as the sample holders which were typically used in the instruments were designed for standard cuvettes. For the PVC cell this was accomplished by screwing a post into the tapped hole on the bottom face of the cell and fitting the post into a holder placed in the proper position within the sample compartment. The ITO cell was held in place using an adapted solid state sample holder which simply pinched the bottom of the cell and held it upright. Once the desired cell was clamped in place of the sample holder it was possible to use the equipment as described in the sections above with almost no differences. However, it was necessary to use a slightly modified set up to excite the sample in the spectroelectrochemical cell for fluorescence measurements as the standard excitation beam is located 90° from the collection lens and the cell is too thin and opaque on the outside edges to allow fluorescence to be emitted from the side face of the cell. By exciting through the front face of the cell at an angle of approximately 45° it was possible to collect fluorescence. This set up is similar to that described above (section 2.3.1) for external excitation using a laser although the sample, in this case, is still excited by the xenon arc lamp.

An EG&G PARC Model 175 universal programmer and a JAS Model JDP 165A potentiostat were used to apply voltage to the spectroelectrochemical cells. The universal programmer was set to cycle between voltages typically using a scan rate of 20 mV/second and a potential window between 0.5 V and -2.0 V. These voltages were selected to function with the solvent used in the system (distilled acetonitrile) while still encompassing the reduction and oxidation peaks of the benzoquinone. Data pertaining to the current flow within the cell was collected from the potentiostat using a National Instruments BNC 2110 data acquisition card along with the National Instruments LabView software (version 7.1).

The potentiostat was connected directly to the cell using alligator clips which made it very difficult to close the sample compartments completely. To avoid light contamination and, potentially, detector saturation it was necessary to run the wires into the sample compartment through the smallest opening possible and use black out cloth to cover these openings.

2.6 Synthesis

A more traditional synthesis of a porphyrin stack system was also attempted. The goal was to link porphyrins with certain characteristics in an H aggregate arrangement by bridging the metal atoms. After consulting the literature, a system which used an oxygen atom as a bridge between porphyrins was chosen as the projected separation between the metal atoms would be close to ideal for intermolecular TTA based on previous theoretical calculations and there was precedent for the reaction. Two relatively simple reactions were found[78,79] that, when combined, resulted in a straightforward two step synthesis for taking the starting materials and converting them to a type of porphyrin polymer.

2.6.1 Materials used

$SnCl_2TPP$ was used as received from Porphyrin Systems. All water used in the synthesis was high purity Millipore water obtained from a standalone system. All other solvents and chemicals were used as received from Sigma-Aldrich.

2.6.2 Synthesis of porphyrin stacks

The first step was the replacement of the axial chlorines with hydroxyl groups to form the dihydroxy compound. 50 mg of 98% $SnCl_2TPP$ was dissolved in 100 mL of Millipore water and 25mL of 99.8% anhydrous pyridine along with 1 g of 99.99% semiconductor grade NaOH. This solution was refluxed for an hour and then allowed to cool. It was then gravity filtered and washed with Millipore water. Once filtered, the solid was left in an oven to dry for approximately 12 hours at 110°C.

The dried product was then placed in a clean reaction flask and heated to 400° C for approximately 20 minutes. A vapour was observed to evolve from the solid within the reaction flask once the flask was placed in the pre-heated sand bath. The product obtained is projected to be the result of a dehydration of the di-hydroxy porphyrin formed in step one. The spectroscopic properties of this product were analyzed to determine its structure.

3. Results

3.1 ZnTPP Studies

ZnTPP is an ideal model compound for dye sensitized solar cells because of its energy absorption profiles and useful photophysical properties. The absorption of red photons (Q band absorption for ZnTPP is ca. 530 nm-630 nm) is necessary for a dye system to take advantage of the photon-rich portion of the solar spectrum and properly utilize TTA within the system.

3.1.1 Steady state absorbance data

Figure 3.1 is a typical example of absorbance experiments performed with the ZnTPP molecule. A solution of the porphyrin was made using aerated toluene (>99.9% purity HPLC grade, Sigma-Aldrich) and successively titrated using freshly recrystallized 4,4-bipyridine (bipy) (Sigma Aldrich) or pyrazine (Sigma Aldrich).

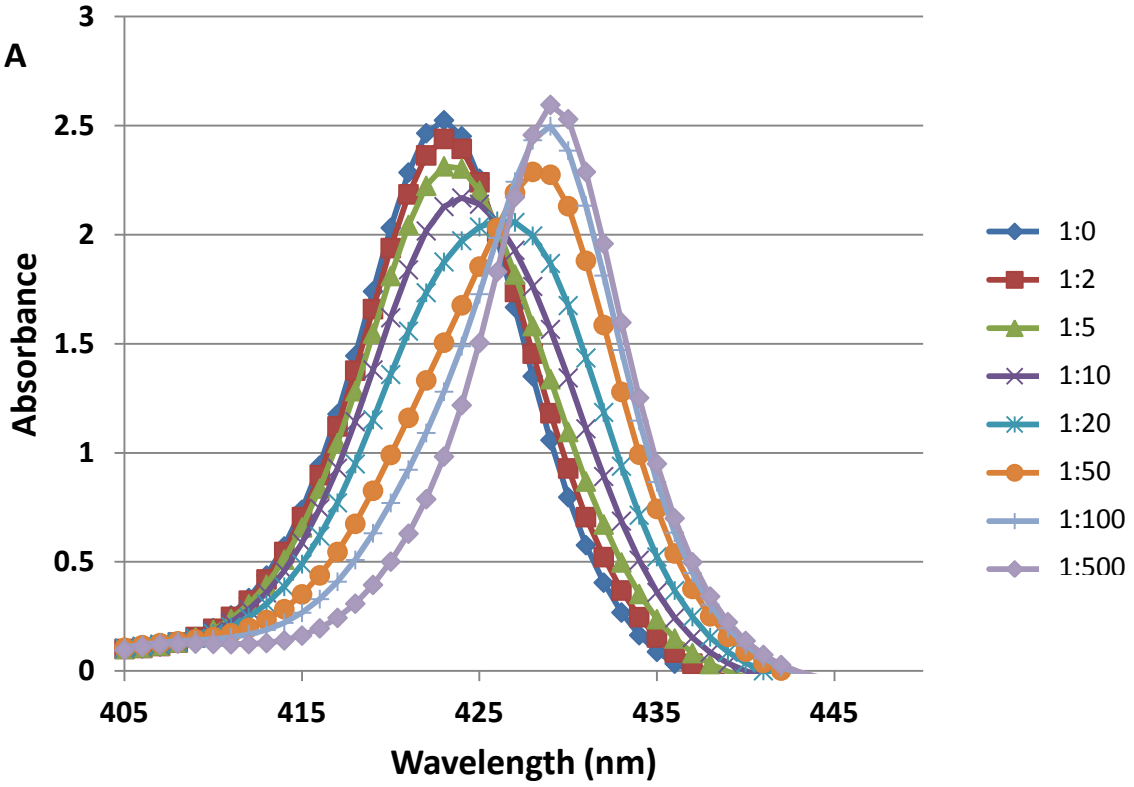

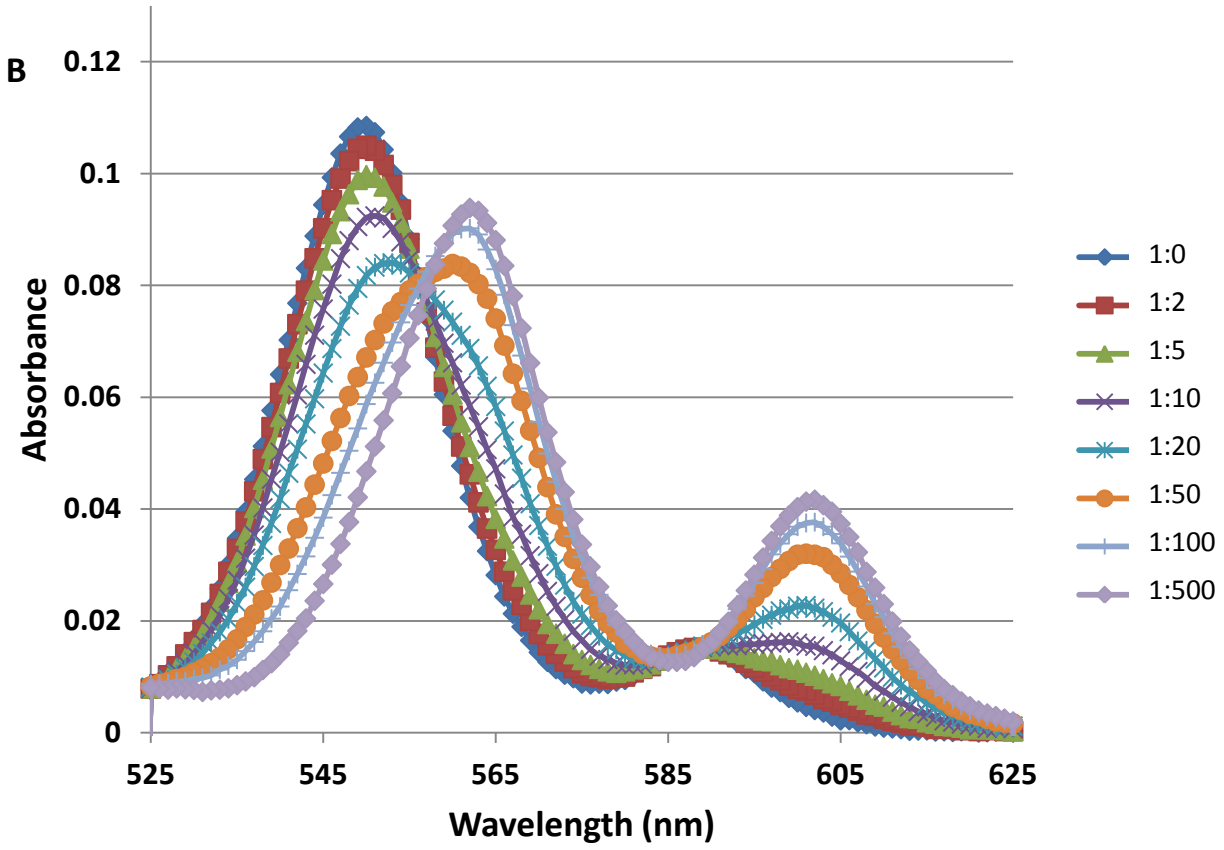

Figure 3.1: Soret band absorption (A) and Q band absorption (B) of 5.0 μM ZnTPP in aerated toluene at 295 K with increasing concentration of bipy (legend gives ratio of concentrations ZnTPP : bipy).

Isosbestic points were observed at 406 & 425 nm in the soret band and at 557 & 591 nm in the Q band. The peak shift of the absorption spectra was quantified and plotted as a means to determine the binding affinity of the bipy for the Zn metal centre of the porphyrin. This was done using a Scatchard plot (figure 3.2) which shows the change in the absorbance of the solution at a given wavelength as a function of the concentration of the ligand in solution.

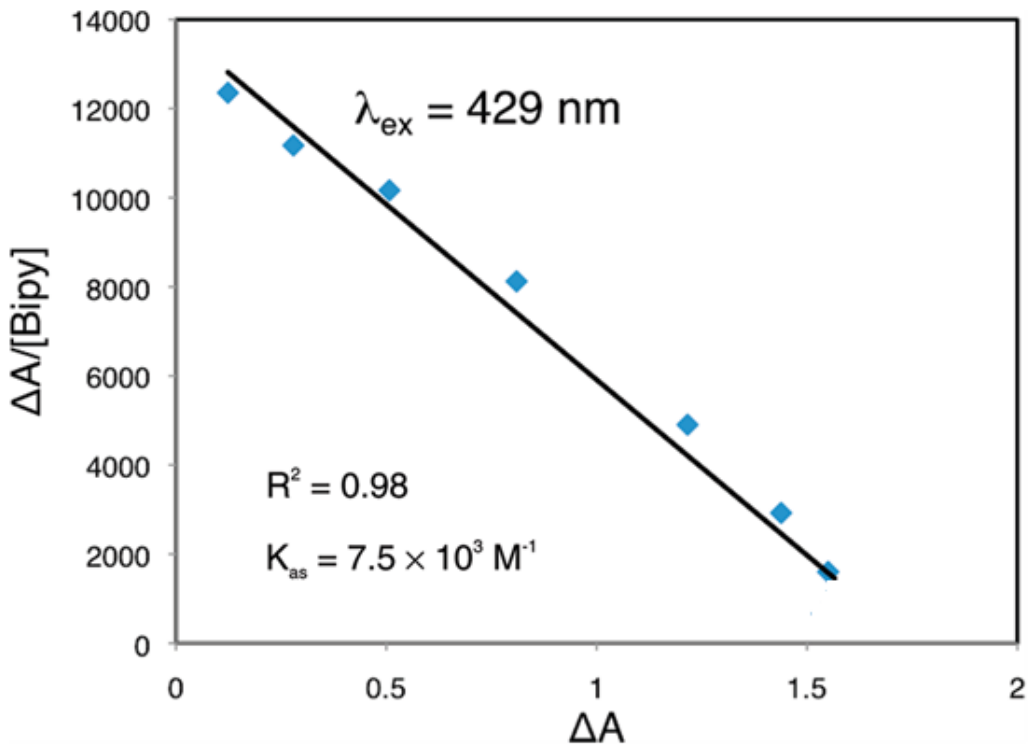

Figure 3.2: Scatchard plot of the titration of a 5.0 μM ZnTPP solution with bipyridine in toluene at 295K. The solution was excited at 429 nm which is the absorption maximum of the ligated species (see figure 3.1). Data for the plot collected by Krysta Bedient.

The Scatchard plot provided the information necessary to determine the association constant (K_{AS}) of the bipy for the ZnTPP using the following expression where ΔA is the change in absorption at 429nm and K_{AS} is the association constant.

$$\Delta A/[bipy]=constant- K_{AS}\Delta A \qquad (3.1)$$

This gives a value for the association of a single ligand with a previously unligated porphyrin. The chances of a second bipy molecule complexing with the metal centre in the ZnTPP molecule was found to be highly improbable particularly at the lower concentrations of ligand that were used in most of this work. Association constants of (7.54 ± 0.25) x 10^3 M^{-1} for the bipy system and (8.8 ± 1.8) × 10^2 M^{-1} for the pyrazine system were measured using this method.

3.1.2 Steady state emission data

Emission data were collected in such a manner as to complement the steady state absorption measurements. By exciting the solutions at an absorption isosbestic point it was possible to remove the necessity of correcting for differences in solution absorbance at the excitation wavelength. When observing the S_2 emission the solutions were excited directly to the S_2 state using a wavelength of 406 nm and for S_1 emission they were excited at 557 nm.

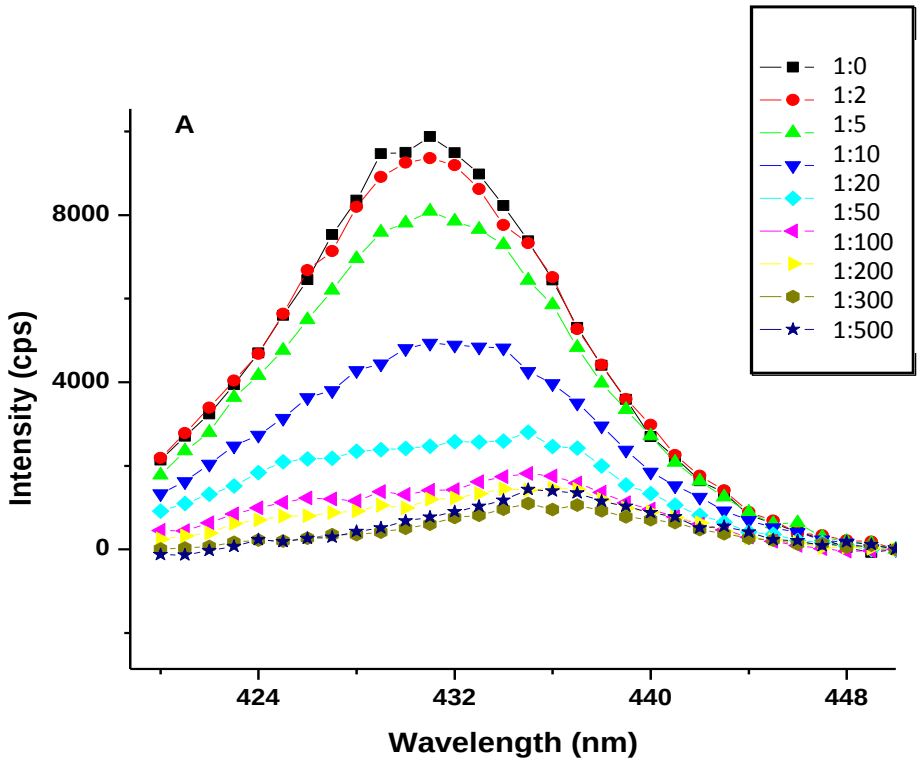

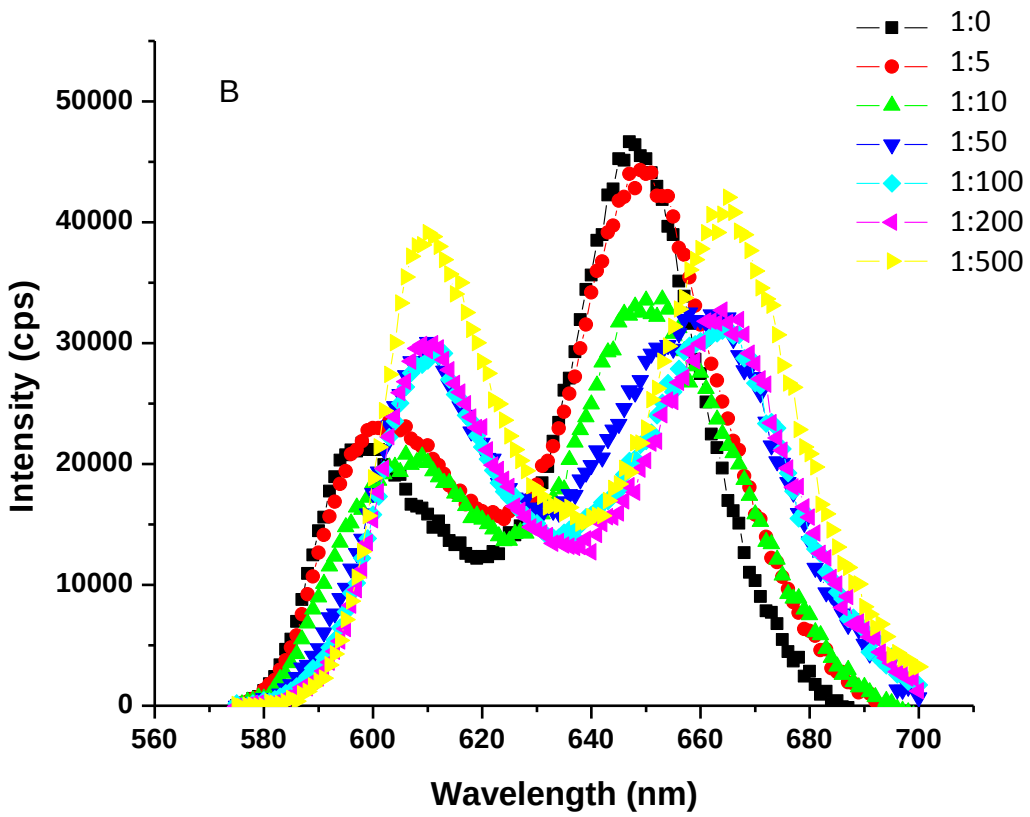

Figure 3.3 Figure (A) shows the S_2 emission spectrum of ZnTPP in aerated toluene with varying concentrations of bipy excited at 406 nm while (B) is the S_1 emission spectra under the same conditions excited at 557 nm. Spectra are not corrected for reabsorption.

The data* show the differences between the emission properties of the ligated and unligated porphyrins. In particular, the bathochromic shift of the S_1 emission peaks is indicative of significant changes to the electronic properties of the molecules upon ligation. In this case the change is due to an increased stabilization of the excited state, due to the attachment of the ligand, as compared to the ground state. This change in the energy gap via ligation does not substantially affect the quantum yield of S_1 fluorescence, however, whereas ligation of ZnTPP by bipy clearly results in quenching of the S_2 emission.

* See Appendix A for similar spectra where pyrazine is used as a linker

3.1.3 Time correlated single photon counting

Once the absorbance data had been collected and an apparent change to the ZnTPP system was observed upon the addition of the ligand, excited state lifetime data needed to be collected to examine whether any effect on the excited state dynamics could be observed.

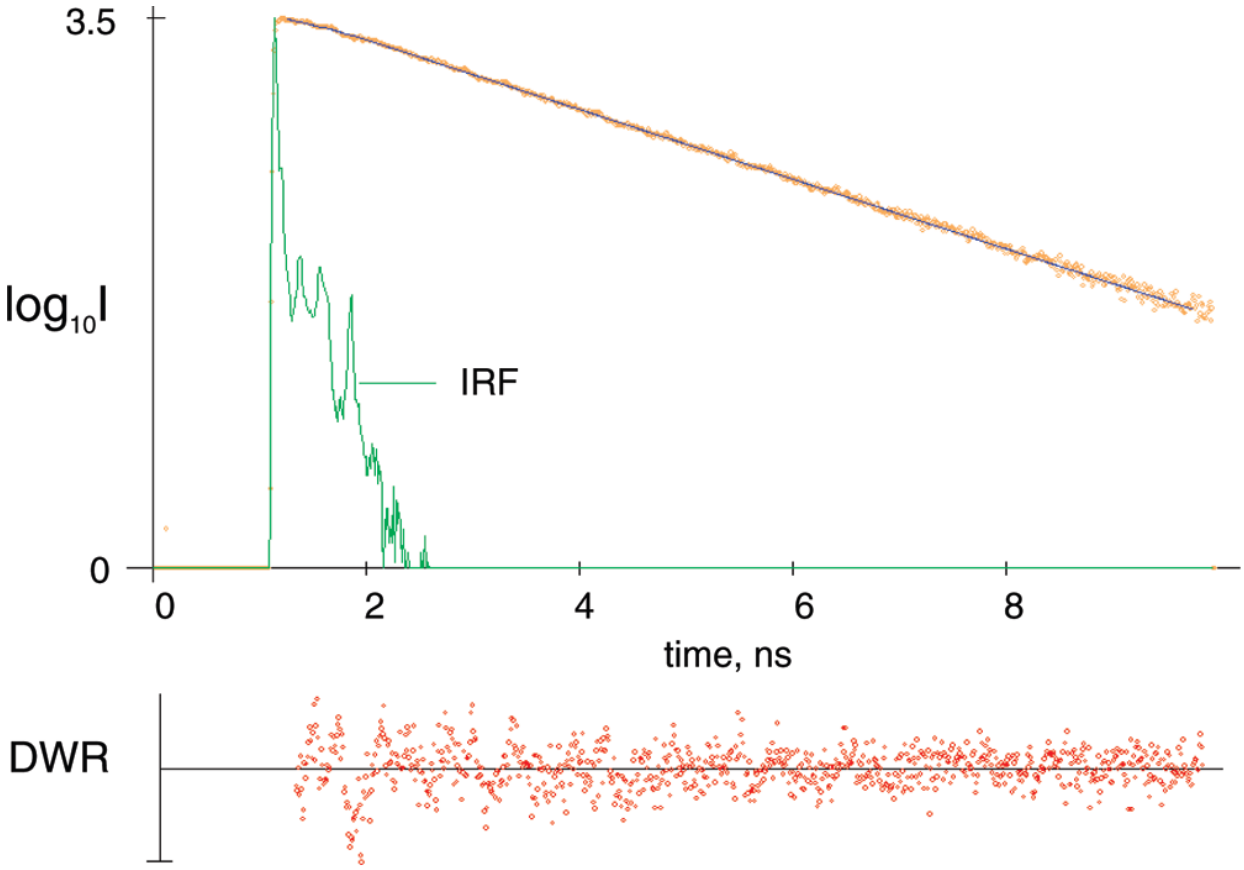

Figure 3.4: S_1 temporal decay for a solution of 5.0 μM ZnTPP and 2.5 mM bipy in toluene. λ_{ex}= 400 nm and λ_{em}= 665nm, the isoemissive point for this system. DWR is the distribution of the weighted residuals with respect to the calculated fit.

The S_1 fluorescence decay shown in Figure 3.4 is typical of the system being studied for this project. Excitation at 400 nm and observation of emission at the isoemissive point (665 nm) ensured that emission from both the ligated and unligated species, if present, would be observed. At large [bipy] : [ZnTPP] ratios the emission data showed that nearly all of the dye species within the sample were ligated. This allowed for direct measurement of the effect

ligation has on excited state lifetimes without having to deconvolute the signal from unligated species. Using the association constant determined from the absorbance data above it was possible to calculate the equilibrium concentration of the ligated species within a sample. The lifetime data for bipy and pyrazine ligated ZnTPP are collected in table 3.1 and show that ligation results in an increasing, though very small, percentage of the excited states decaying through a substantially faster route than for the unligated species.

Table 3.1 S_1 temporal fluorescence decay parameters for 5.0 μM ZnTPP in toluene with varying concentrations of pyrazine and bipyridine[a].

	([ZnTPP]/[ZnTPP]$_0$)	τ_1, ns	τ_2, ns	F_1	F_2
[pyrazine], μM					
0	1.00	1.99	0	1.00	0
10	1.00	1.99	0	1.00	0
25	0.98	1.99	0	1.00	0
50	0.96	1.99	0.11	0.99_9	0.001
250	0.82	1.98	0.14	0.99_6	0.004
1000	0.53	1.97	0.32	0.98_8	0.012
2500	0.31	1.89	0.21	0.99_7	0.003
[bipyridine], μM					
0	1.00	1.99	0	1.00	0
10	0.93	1.98	0.21	0.99_7	0.003
25	0.85	1.97	0.21	0.99_4	0.006
50	0.74	1.96	0.21	0.99_2	0.008
250	0.35	1.82	0.21	0.99	0.010
1000	0.12	1.70	0.16	0.99	0.011
2500	0.05	1.65	0.19	0.99	0.011

Pyrazine-ligated ZnTPP samples were excited at 475 nm and bipyridine-ligated samples were excited at 400 nm. Fitting data was obtained using the equation $I(t) = \Sigma\, a_i \exp(-t/\tau_i)$ where τ_i is the lifetime. F_i is the percentage of the emission that each component contributes ($F_i = a_i\tau_i/\Sigma\, a_i\tau_i$) and ($[ZnTPP]/[ZnTPP]_0$) represents the calculated fraction of unligated ZnTPP present in the sample. [a] Nanosecond lifetimes have an average error of ±0.02ns and subnanosecond lifetimes have an average error of ±0.06 ns.

3.1.4 Fluorescence upconversion data

In order to obtain information concerning the S_2 decay profile and the S_1 rise time following Soret-band excitation, fluorescence upconversion measurements of the ZnTPP-ligand systems were taken. Typical data for both types of measurements can be seen in figure 3.5 where the solid line represents the calculated fit and the dots are the collected data.

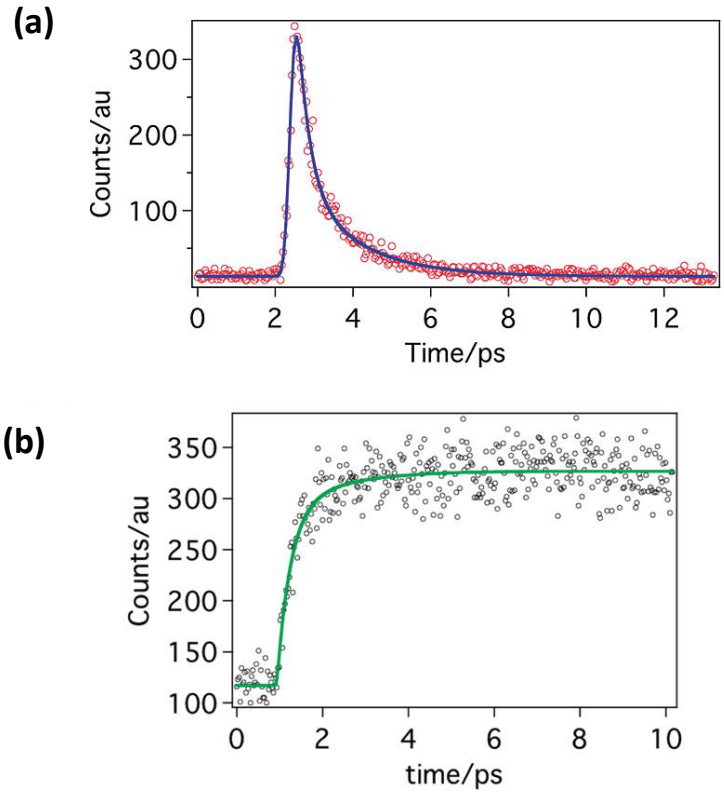

Figure 3.5 (a) S_2 temporal fluorescence decay for 150 µM ZnTPP and 600 µM bipyridine in toluene using λ_{ex} = 400 nm and λ_{obs} = 433 nm. (b) S_1 fluorescence rise profile for 150 µM ZnTPP and 600 µM bipyridine in toluene using λ_{ex} = 400 nm and λ_{obs} = 654 nm. Data collected and fit by Dr. Manisankar Maiti.

Each sample was measured a number of times and the data obtained (table 3.2) were all averages of between three and five measurements. A concentration of 150 µM ZnTPP was needed to get satisfactory signal to noise for the upconversion measurements which, while substantially greater than in the other measurements, has been shown[60] to have no significant effect on the excited state dynamics when solvated in a non-coordinating solvent. This was important as higher concentrations increase the likelihood of aggregation of the ZnTPP molecules which can allow more non-radiative decay pathways from excited states.

Table 3.2 S_2 temporal fluorescence decay parameters for 150 µM ZnTPP in toluene with varying concentrations of pyrazine and bipyridine using a biexponential fitting function. Data collected by Dr. Manisankar Maiti.

	$[ZnTPP]/[ZnTPP]_0$	τ_1, ps	τ_2, ps	F_1	F_2
[pyrazine], mM					
λ_{ex} = 400 nm					
0	1.00	1.47± 0.02	0	1.00	0
7.5	0.13	1.49± 0.02	0.29±0.02	0.66±0.04	0.34±0.04
150	0.00	not obs.	0.28 ±0.04	0	1.00
[bipyridine], µM					
λ_{ex} = 400 nm					
0	1.00	1.48±0.02	0	1.00	0
300	0.39	1.50±0.04	0.24±0.02	0.80±0.10	0.20±0.10
600	0.22	1.51±0.05	0.29±0.02	0.63±0.10	0.37±0.10
2000	0.07	1.54±0.22	0.22±0.04	0.44±0.16	0.56±0.16

These data show that as an increasing fraction of the ZnTPP is ligated the S_2 excited state of the ligated species undergoes much faster decay than the unligated molecule. The S_2 lifetimes for the unbound molecule correspond closely with previous studies[60,80] and the decrease in the lifetime of the ligated molecules matched well with the steady state emission data shown in

figure 3.3. The S_1 rise time of the ZnTPP-Bipyridine system was measured and was found to be identical to the S_2 decay time within an error of ± 15%. The relatively large error in this measurement is due to a much faster radiative decay rate which leads to a lower count rate and in turn a much lower signal to noise ratio (Figure 3.5 b). In the unligated system the rise time of the S_1 state, when excited in the Soret band, is equal to the S_2 decay rate as the conversion efficiency between the two states is nearly unity (*cf*. section 4.4). For the purposes of this analysis it was considered as constant when compared to the effects of ligation on the S_2 lifetimes and the subsequent photophysical changes that this created within the system. Furthermore, the fact that there is no significant change in the S_1 rise time means that any additional states in the S_2 decay pathway are very short lived (< 150 fs).[56]

3.2 $SnCl_2TPP$ studies

After investigating the effects of ligation on the ZnTPP molecule it was observed that the Zn metal centre was unlikely to form more than one axial coordinate covalent bond, which was later corroborated by the literature.[81] This difficulty arises from the fact that the formation of an axial coordinate covalent bond between the metal and a ligand pulls the Zn atom out of the plane of the porphyrin ring. This leads to a much larger hindrance for any ligand trying to coordinate to the Zn from the other side of the ring as it must now effectively overcome a substantial steric hindrance to approach the metal. As our intention was to create sandwich type molecules and eventually look at longer column type molecules this presented a problem. Since the $SnCl_2TPP$ molecule already possesses two axial bonds it was used for further studies in the hope that the two chlorine atoms could simply be displaced by other ligands which can then be used to create the desired supramolecular structures.

3.2.1 Synthesis results

The two approaches to synthesis (electrochemical and dehydration) of a Sn porphyrin stack were very different and yielded inconsistent and inconclusive data. The electrochemical synthesis gave more concrete data about what was actually occurring in the system during the synthesis as it was done in a more systematic and controlled manner. Cyclic voltammograms (CV) were created both before the benzoquinone was present in the system (blank) and again

once the benzoquinone had been added. The reduction and subsequent oxidation of the benzoquinone is evident in the CV below. It appears as two downward peaks (reduction) between -1.15 V and -1.40 V followed by two upward peaks (oxidation) between -1.00 V and -1.30 V.

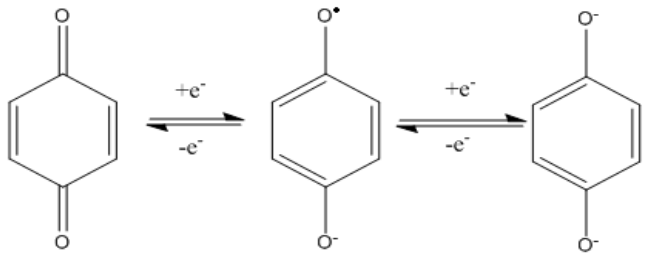

Scheme 3.1 Reduction of benzoquionone

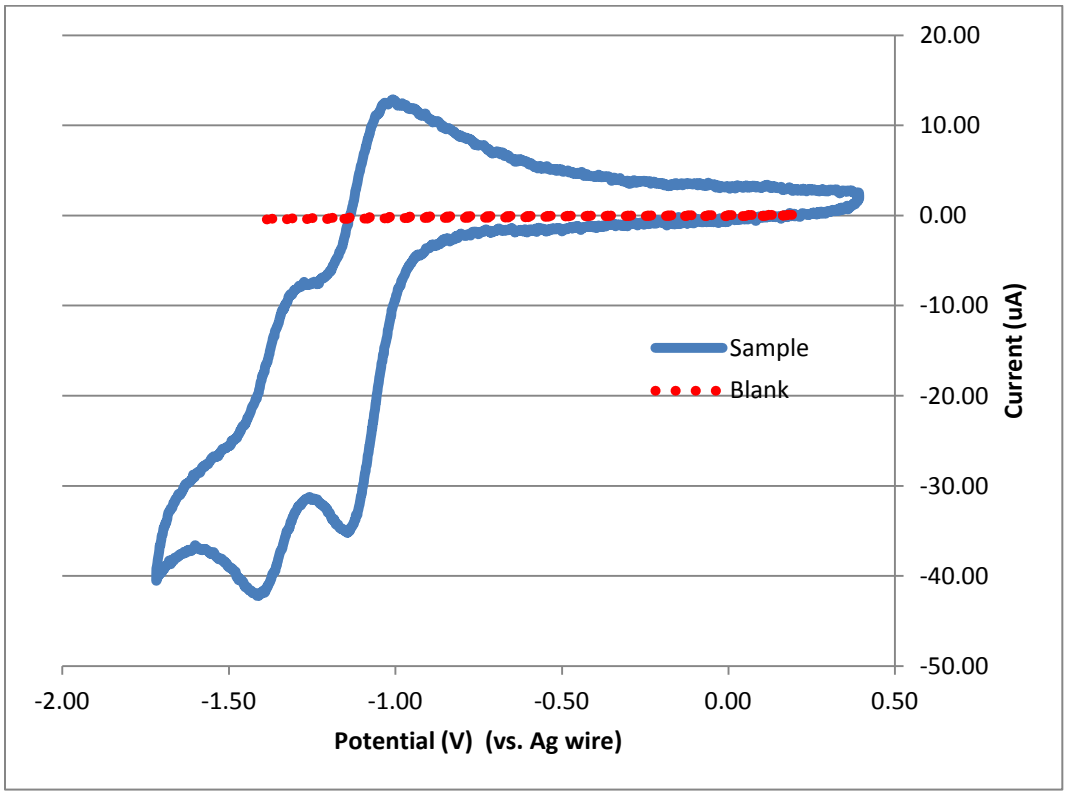

Figure 3.6 Cyclic Voltammogram of a blank and the double reduction of Benzoquinone in dry acetonitrile, measured against a silver wire.

By holding the cell at a negative potential relative to the second reduction peak it was possible to convert a large amount of the benzoquinone (nearly all of it in the small volume cells) to the doubly reduced form. Because ligands containing electron rich oxygen atoms are known[82] to have a high affinity for the Sn atom within the porphyrin, it was anticipated that they would quickly bind to a porphyrin upon reduction and that they would also be able to bind another porphyrin with their second oxygen creating a sandwich compound.

3.2.2 Absorbance and Raman spectra

By taking absorbance measurements of the solutions before and after the creation of stacked porphyrin arrays was attempted, a method for determining what changes, if any, had taken place within the system was devised. The absorbance scans of the two different solutions reveal that the product of the electrochemical synthesis has peaks which are blue shifted compared to the starting materials and there has also been a change in the relative intensities of the peaks, particularly in the Q band. The wavelength shift in the peaks is on the order of 3 nm, which is relatively large compared to the bandwidth used and the error in the spectrophotometer.

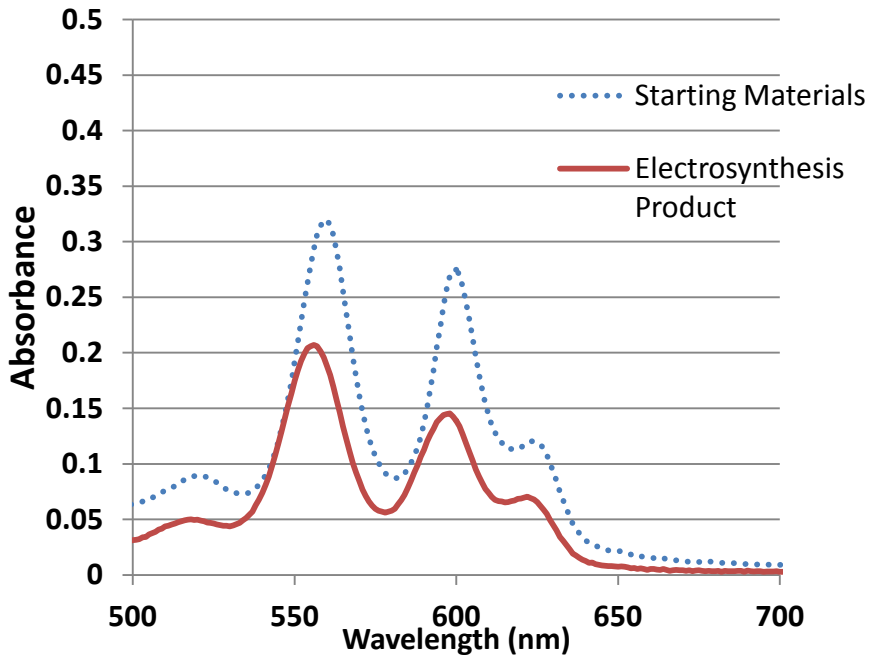

Figure 3.7 Absorbance of a solution of $SnCl_2TPP$, benzoquinone and tetrabutylammonium hexafluoroborate in distilled (dry) acetonitrile before and after the electrochemical reduction of the benzoquinone.

While the changes in the absorbance spectra indicated that something had taken place, they did not give definitive proof that the desired product had been obtained. Further electrochemical synthesis experiments were performed in an effort to gain more substantial evidence for the nature of the product. During one of the electrochemical experiments where gold was used as the working electrode a solid was deposited onto the gold surface. This solid was examined using a Raman microscope and compared to Raman spectra of the starting materials used. In much the same way as the absorbance spectra for the starting materials were used as a background, Raman spectra of the individual starting materials were taken and combined to create a spectrum that the product could be directly compared to.

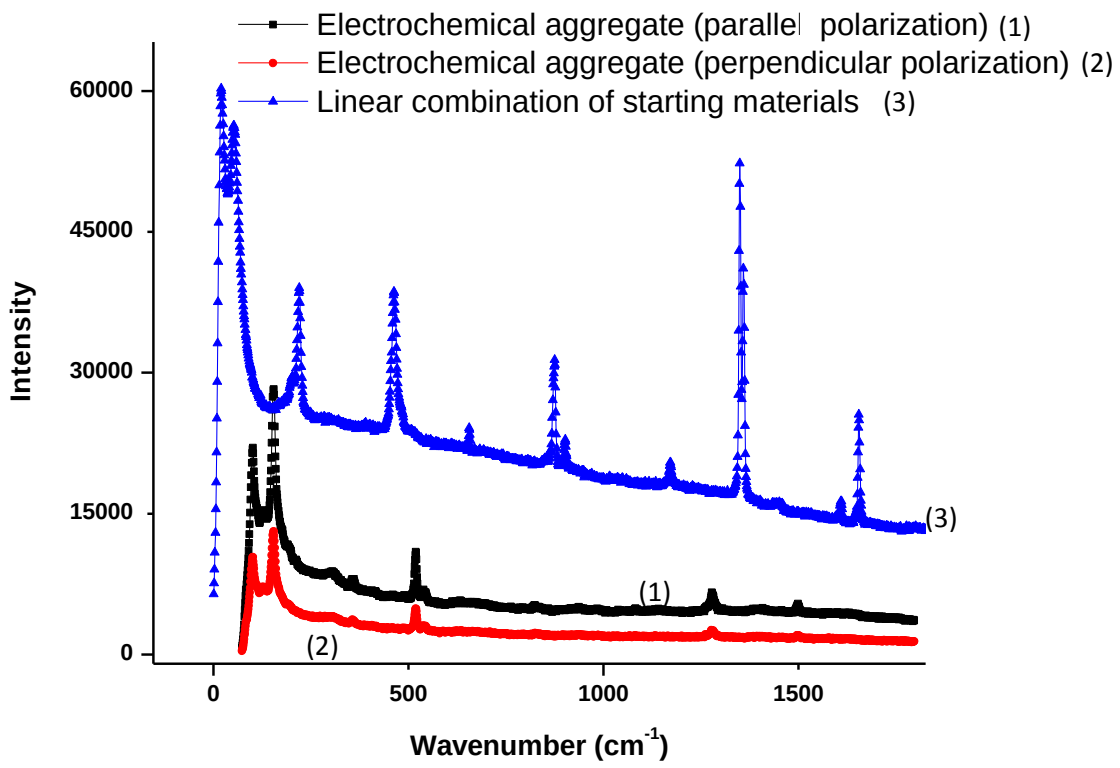

Figure 3.8 Raman spectra of the aggregate formed on the gold working electrode as compared to a sum of the Raman spectra of the starting materials. Data collected by Jason Maley of the SSSC.

Literature values were used to identify the observed peaks that were considered most important for the identification of the changes that occurred during the synthesis. Particular interest was given to strong bands that were present in the starting materials but absent or shifted significantly in the product.

Table 3.3 Raman band assignments for starting materials and products of electrochemical synthesis.[81-83] In the Assignment column Q is indicative of a quinone stretch P of a porphyrin stretch.

Starting materials band (cm^{-1})	Product band (cm^{-1})	Assignment
1654	N/A	C=O vibration (Q)
1596	N/A	Phenyl ring (P)
1536	N/A	C=C stretch (P)
1483	1499	C=C stretch (P)
1454	N/A	C-C stretch (P)
1395	N/A	C-C stretch (Q)
1367	N/A	C=N stretch (P)
1245	1278	Phenyl ring (P)
1151	N/A	C-H stretch (Q)
771	823	Ring Breathing (Q)
N/A	538	Sn-O stretch (?)
N/A	519	Sn-O stretch (?)
442	N/A	In plane ring deformation (Q)

One of the most significant pieces of data obtained from the analysis of the Raman spectra was the obvious loss of the very strong carbonyl stretch from the benzoquinone. This may be the result of a bond being formed between the Sn metal centre and the oxygen of the quinone. Another significant piece of information were the bands near 500 cm^{-1} which correspond closely to Sn-O stretches reported in the literature.[83] A more general observation is the dramatic decrease in the number of bands visible in the spectrum of the product which typically indicates a change in the symmetry of the molecule.

Once the electrochemical synthesis had been completed, an attempt at a more traditional synthetic approach was undertaken. The goal of this synthesis was again a stacked porphyrin

structure but in this case the spacer between the individual porphyrin units would be much smaller than that of the electrochemical synthesis. A synthetic procedure was devised (*cf.* Section 2.6) for linking two porphyrins together using an oxygen atom.

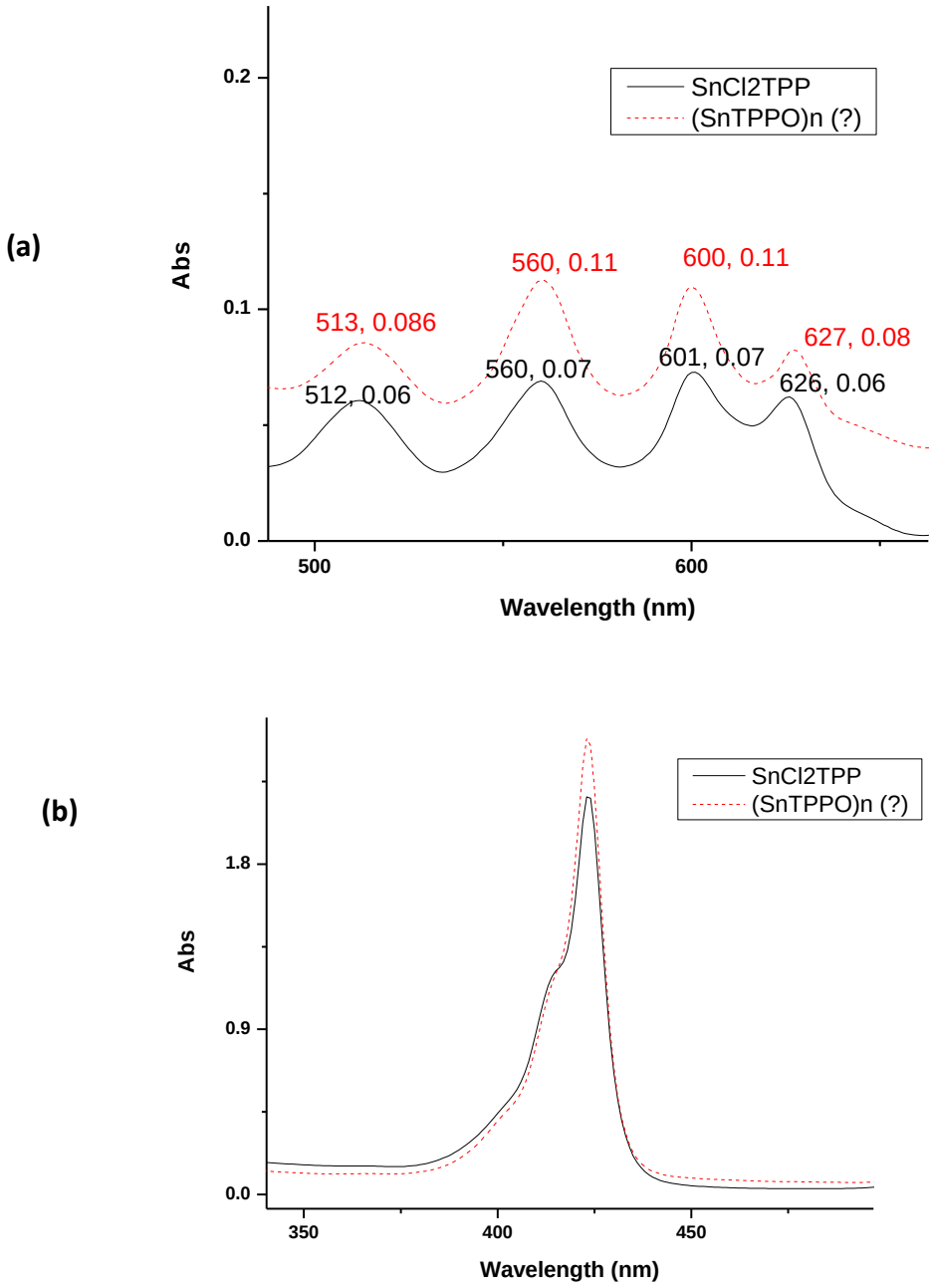

Figure 3.9 (a) Q band and (b) B band absorption spectra of the synthesized product and starting material.

Upon examination of the absorbance spectra obtained it was clear that there were some minor changes that could be indicative of a product. The most significant changes were those that took place in the Q band where there was a shift in the separation of the two peaks furthest to the red as well as a change in their relative intensities. There was also a significant change in the shape of the Soret band where the shoulder on the blue side of the band seems less defined than in the $SnCl_2TPP$. While these may seem like small changes, absorbance spectra are not particularly sensitive to the types of changes anticipated therefore any differences that are observed could indicate large modifications to the molecular structure.

3.2.3 Emission spectra and lifetime measurements

Emission spectra of the stock $SnCl_2TPP$ in anhydrous acetonitrile were taken and compared to a sample of the product from the intended oxygen-linker synthesis, which will be called (SnTPPO)n herafter for the sake of convenience.

(a)

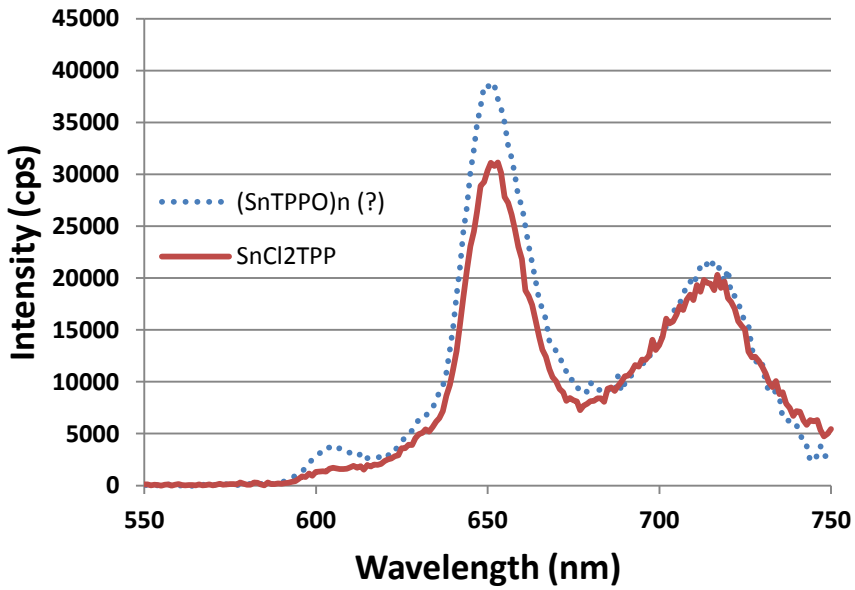

(b)

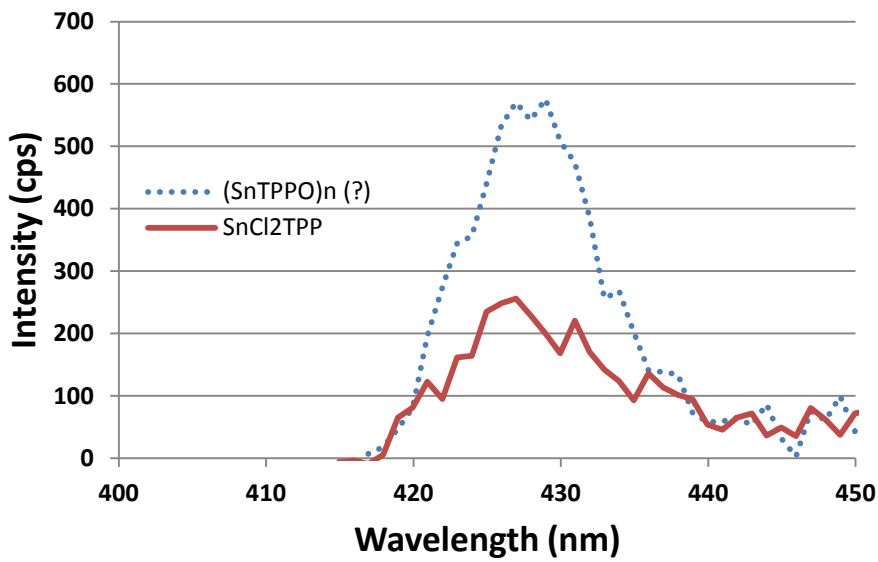

Figure 3.10 (a) S_1 and (b) S_2 steady state emission of $SnCl_2TPP$ and (SnTPPO)n (?), excited at 400 nm.

S_1 lifetime data for both of these products were also obtained for excitation both into the Soret and Q bands.

Table 3.4 TCSPC S_1 lifetime data for $SnCl_2TPP$ and (SnTPPO)n in anhydrous acetonitrile [a]

	λ_{ex} (nm)	τ_1, ns	τ_2, ns	F_1	F_2
$SnCl_2TPP$	410	9.09	0.75	0.98	0.02
	498	7.55	0.40	0.80	0.20
(SnTPPO)n	410	9.28	0.60	0.97	0.03
	498	7.65	0.41	0.75	0.25

[a] Nanosecond lifetimes have an average error of ±0.02 ns and subnanosecond lifetimes have an average error of ±0.06 ns.

4. Discussion

4.1 Factors determining energy transfer rates

In order to apply the information that has been collected and determine whether porphyrins are viable as potential DSSC light harvesting substances it is important that the factors affecting energy transfer within the system be understood. In porphyrins intramolecular radiationless decay processes compete with intermolecular processes because their electronic states tend to correspond to the weak coupling limit (*cf.* section 1.8). This means that radiationless transitions within the molecules studied in this work obey the energy gap law which will assist in understanding their relaxation pathways. The relatively large energy gap between the S_2 and S_1 states results in a slower rate of non-radiative internal conversion allowing for fluorescence from the S_2 to the S_0 state which is observable in the steady state and time-resolved emission spectra.

4.2 General effects of ligation

When analyzing the data obtained for the ligation of the ZnTPP molecule, the first consideration is the ability to form a coordinating bond between the ligand and the metal atom. It has been known for some time[84] that the Zn atom has a relatively strong affinity for N and O containing ligands which have the ability to act as strong electron donors. Our data (*cf.* Figure 3.2) shows a binding constant for bipyridine of $(7.54 \pm 0.25) \times 10^3$ M^{-1} which is large enough that ligation is likely to take place when an excess of the ligand is present but not so large as to expect a second ligand to coordinate to the Zn, particularly as the first ligand tends to pull the metal centre out of the plane of the ring. The displacement of the metal atom makes it difficult for ligands to access the Zn as the ring will essentially act as a large steric hindrance to molecules approaching from the unligated face. However, it may be possible to promote the formation of a second metal-ligand bond in cases where the concentration of the ligand is significantly greater than that of the porphyrin (i.e. [ZnTPP] : [bipy] = 1: 2500).

The formation of the porphyrin-ligand complex stabilizes the electronic states of the porphyrin, with the excited states undergoing stabilization to a greater extent than the ground state which

leads to a diminution in the energy gaps between these states. These energy gaps can be measured by simply analyzing the absorbance spectra of the ligated and unligated species. The energy gaps between the ground state and the S_2 and S_1 states decreased by 400 cm^{-1} and 300 cm^{-1} respectively when the ZnTPP was complexed with bipyridine. This change in the energy gap between the ground state and excited states is what leads to a red shift in the spectrum, which is readily observed even at low ligand concentrations (*cf.* figure 3.5). Ligation of the central metal atom would appear to generate this bathochromic shift because of its effect on the bonds within the porphyrin macrocycle as well as the distortion of planarity due to withdrawing the Zn from the central cavity.[85] The distortion of bonds allows for the extension of the π-system into the aryl groups in the meso position of the porphyrin ring which in turn reduces the energy of the various states the porphyrin may occupy. This shift in energy does not have a significant effect on the rate of S_1 fluorescence, partially because there is a very small change in the energy gap between the S_1 and T_1 states which (according to the energy gap law) means there should be a relatively small change in the rate of $S_1 \rightarrow T_1$ intersystem crossing which is the primary relaxation pathway.

Other changes that are observed in the S_1-S_0 absorption spectra (*cf.* Figure 3.1) upon formation of a non-covalent coordinating bond between the Zn and ligand are the changes to the relative intensity of the 0-0 and 0-1 bands. This change is due to the change in the overall symmetry of the molecule upon addition of the ligand. The transition from a D_{4h} to a C_{4v} symmetry alters the conditions which restrict the 0-0 transition. When the molecule has a D_{4h} symmetry the transition from a v=0 state to another v=0 state is hindered and most of the signal that is observed occurs through intensity-borrowing via symmetry breaking vibrations. This means that vibrations occur which break the D_{4h} symmetry thereby allowing a 0-0 transition to take place. However, once the symmetry of the system is changed to C_{4v} there is no need to break the symmetry of the molecule for these transitions to take place therefore the probability of a transition occurring and the intensity of the related spectral peak increases. The same logic applies to the changes in relative peak intensities in the emission spectra.

Another factor to be considered is the separation between porphyrins that can be created by an axial ligand. Figure 4.1[57] demonstrates that axial ligation of porphyrins can cause a significant decrease in the occurrence of TTA by creating a physical barrier to intermolecular approach of the two triplets (*cf.* 1.6). If a ligand were found that had a very high ligand-porpyrin binding constant it may be possible to promote the formation of sandwich complexes which could increase the rate of TTA by preventing the diffusion of porphyrins away from each other. However, even if such a ligand were found it would also need to be very small, so as to allow orbital overlap between the dyes, or it would have to provide a means to electronically connect the two sets of π orbitals. As any system acting as a linker tends to be orthogonal to the π systems of the dyes it seemed the best path to try using a very small linker, which led to the attempted synthesis of the Sn porphyrin stacks that are linked simply by an oxygen atom.

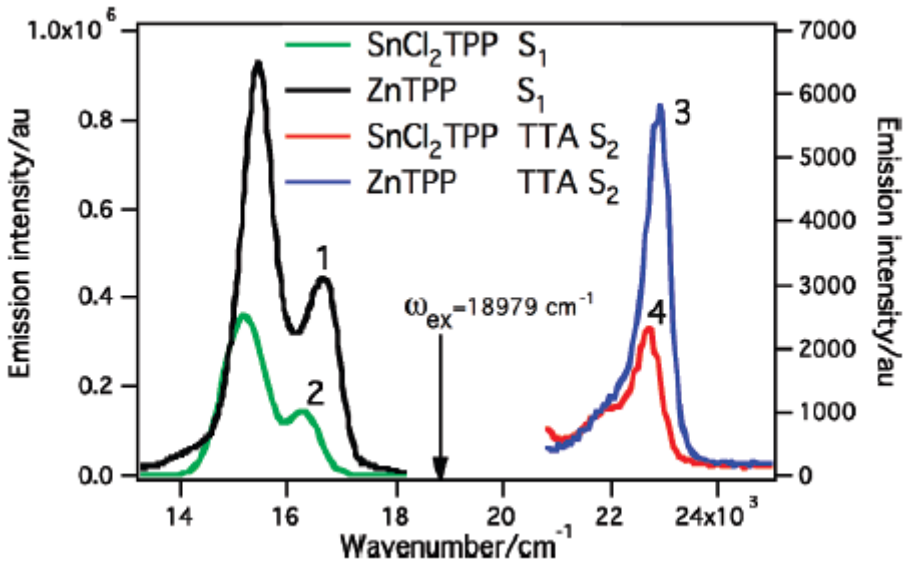

Figure 4.1 S_1 and delayed S_2 emission from ZnTPP (1&3) and $SnCl_2TPP$ (2&4) excited at 18979 cm^{-1}. Both solutions were adjusted so that their absorption at ω_{ex} was equal, emission has been normalized but ZnTPP exhibited TTA 220 times as intense as that observed from the $SnCl_2TPP$[57].

The last difference between the ligated and unligated species to discuss when looking at ZnTPP as a potential dye system for DSSC applications is the affect ligation has on the S_2 lifetime. By comparing the S_2 emission of the two systems it is easy to see that the act of ligating the dye

has an effect on the S_2 state as fluorescence from the Soret band is essentially nonexistent in the ligated species (figure 3.5). By examining the behaviour of the ligated porphyrin in other studies done in various liquid solvents[60,86] it becomes clear that the rate of fluorescence from the S_2 state is essentially constant, irrespective of whether the dye is ligated or not. Since this is the case the only explanation for a reduction in fluorescence must be an increase in the ability of the dye to lose energy through additional non-radiative pathways. To measure whether or not there is a significant change between the decay pathways of the ligated and unligated species two sets of time-correlated data pertaining to the S_2 lifetime were obtained. The data show that ligated ZnTPP has a much shorter S_2 lifetime than the unligated species (approximately 250 fs vs. 1.5 ps) which, as discussed in 1.5.2, can significantly decrease the ability of a dye to inject an electron into a semiconducting surface. The mechanism for this quenching is of interest as it may give insight into whether the kinetics of electron transfer from the excited state to the semiconductor will be affected, as well as providing information on what characteristics the ligands possess that promote this quenching. We can immediately exclude electronic energy transfer (EET) as a mechanism since the S_1 excited states of both ligands have electronic energies that are higher than the S_2 state of the porphyrin making them inaccessible.

4.3 Excited state dynamics of ligated species

S_1 decay times show that there is virtually no difference between the rate of decay for the ligated species versus that of the unligated species. Although small differences in the lifetimes seem to grow as the concentration of ligand is increased (table 3.1) the differences remain relatively small and account for a minor percentage of the total decay. These changes in S_1 lifetime are so small, when compared to the changes observed in the S_2 dynamics, that it is apparent that the mechanism by which the S_2 state is being quenched has no significant effect on the S_1 state.

Studies of the S_1 rise time reveal that, within error, it follows the S_2 decay lifetime whether the ZnTPP molecule is ligated or not. Unfortunately because of the relatively low radiative decay rate (compared to S_2) and in turn the low count rate, measurements of the S_1 rise time have an

error of approximately 15%, mostly caused by higher background noise contributions that accumulate over the measurement period. Because of this large error, it is difficult to say whether the S_1 rise follows the S_2 decay exactly but since the conversion efficiency between the two singlet states remains at or near 100% (*cf.* 4.3) we know that the transition from the S_2 to the S_1 state cannot occur via intermediate state with a significant lifetime (i.e. > 300 fs).

One explanation for the change to S_2 properties could be the change in the symmetry. It is possible that by converting the molecule from a D_{4h} to a C_{4v} symmetry, via ligation, a change to the potential surfaces of the molecule have been affected as well. In an unligated porphyrin the S_1 and S_2 potential surfaces are situated in such a way that they exhibit weak interstate coupling. This weak interaction leads to picosecond lifetimes for the S_2 state and a system that obeys the energy gap law. However, it is possible that ligation of the porphyrin could shift the S_2 potential surface relative to the S_1 surface such that they exhibit strong interstate coupling. If this were to occur the system would display surface crossing between the two states and S_2 lifetimes in the femtosecond timescale. Although this appears to fit our experimental data well, other experiments[60,80,87] involving axial coordination of a ligand (i.e. pyridine, DMF, THF etc...) with a metallated porphyrin do not exhibit such behaviour even though they cause the same change in symmetry as ligation with bipyridine and pyrazine. It became necessary to examine the decrease in the quantum yield of S_2 fluorescence as well as the shortened S_2 lifetimes (table 3.2) when the porphyrin was coordinated to these two ligands in light of this contradicting information. Upon closer analysis it was discovered that differences in the redox properties of the ligands will affect whether or not radiatonless S_2 decay by intramolecular electron transfer takes place. In the bipyridine and pyrazine systems this type of decay is evident but it does not occur in the other ligands that have been studied, such as pyridine.

4.4 Energetics of electron transfer

For efficient electron transfer to take place between the porphyrin and the ligand it is necessary for the value of ΔG_{ET}, as calculated using the Rehm-Weller model (section 1.6), to be negative. This is the case for ET from a porphyrin excited in the Soret band for both pyrazine and

bipyridine although the bipy shows a stronger driving force for ET than the pyrazine, as seen in Table 4.1.

Table 4.1 Electron transfer parameters for Soret excited ZnTPP:L in toluene (adapted from [56])

Ligand	E_{ox} (V vs. SCE)	E_{red} (V vs. SCE)	E^* (V)	ΔG_{ET} (eV)
pyrazine	0.86 max			0.13 max
	0.79 best	-2.17	2.90	0.06 best
	0.50 min			-0.23 min
bipyridine	0.86 max			-0.12 max
	0.79 best	-1.91	2.89_1	-0.19 best
	0.50 min			-0.48 min
pyridine	0.86 max			0.72 max
	0.79 best	-2.76	2.90	0.65 best
	0.50 min			0.36 min

Half-wave potentials were obtained by performing cyclic voltammetry experiments in dichloromethane which contained 0.1 M tetrabutyl ammonium salts as an electrolyte. The reported values give the range of voltages obtained (max and min) for different anions in solution. The best value is based on measurements performed when anions (e.g. perchlorate, tetrafluoroborate etc...) that do not complex with ZnTPP were used. All potentials were measured vs. SCE.

Since the ligand is bound to the porphyrin this allows for intramolecular electron transfer which, like many intramolecular processes, can occur at a much quicker rate than intermolecular electron transfer. In this case the ability to forego the ion separation and solvent reorganization steps leads to a very fast transfer. The transfer is further facilitated by the fact that these compounds are being excited at a wavelength that produces a vibrational state slightly higher in energy than the zeropoint level of the Soret band, this means that the S_2 states initially have added thermal energy which facilitates ET. From the S_2 emission data we know that this charge transfer from the porphyrin to the ligand takes place on a time scale of approximately 200 fs and it would stand to reason that the reverse process, transfer from the charge separated species back to the porphyrin (S_1 state), could occur on the same time scale.

We have shown that the overall process must occur on a relatively short time scale. This is confirmed by measurement of the net S_2-S_1 internal conversion efficiency, which is nearly unity for both the ligated and the unligated species, as shown in Figure 4.2.

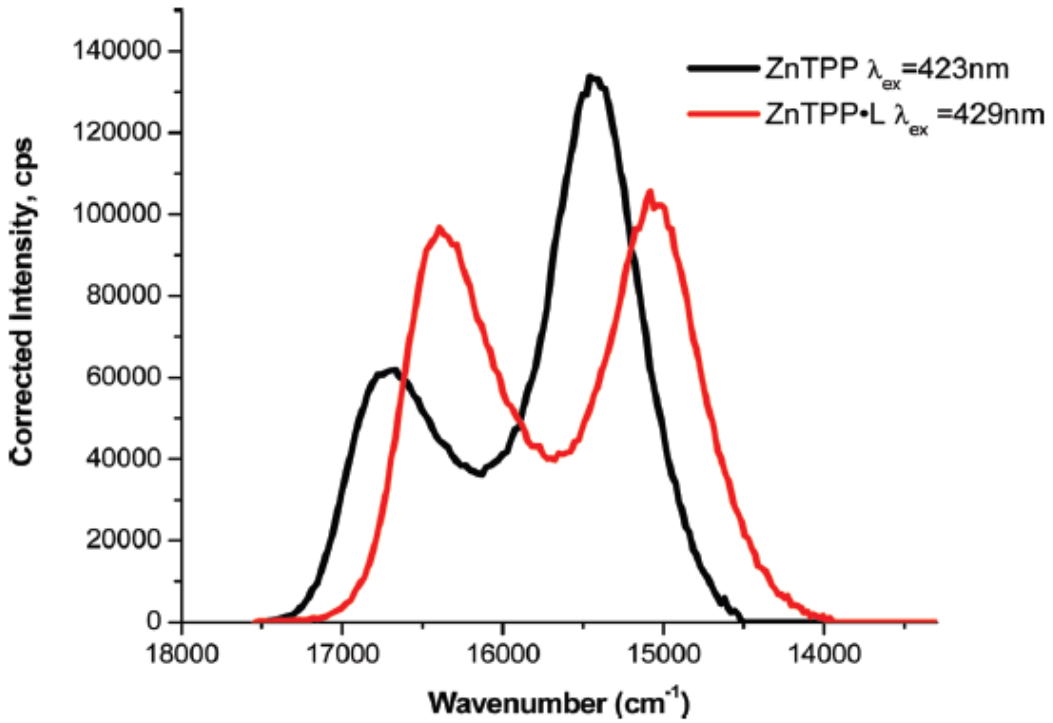

Figure 4.2 Corrected S_1-S_0 emission spectra for ligated and unligated ZnTPP. Both were excited at their respective Soret band maximum and corrected for absorbance, detector and lamp variances with wavelength.

The ratio of the integrated intensities of the S_1 emission was found to be ZnTPP·L : ZnTPP = 1.07:1 with an estimated error of ±0.10. This indicates that there is no significant difference in the net internal conversion efficiency from S_2 – S_1 between these species and the charge recombination after the creation of the charge transfer state must necessarily be fast (fs time scale).

4.5 Synthesis of porphyrin stacks

In an effort to create systems that had higher TTA efficiency and in turn higher overall efficiency as a potential energy harvesting system, synthetic means of creating supramolecular porphyrin structures were pursued. Though there was difficulty when attempting to definitively

determine the nature of the products created using these synthetic procedures, there seems to be some evidence as to what was created and what kind of photoproperties it may possess.

When performing the electrochemical synthesis with a potential benzoquinone bridging ligand it was crucial to ensure that the proper species in solution was being reduced. Once literature redox values for the porphyrin were found[88] it was evident that the benzoquinone was the species that was undergoing reduction. The differences in the UV-visible absorption spectra were clearly present but they were not very dramatic. However, the sensitivity of absorbance measurements with regard to the expected types of structural differences between the desired product and the starting materials is not very high. A blue shift of the absorption peaks as well as a drop in the peak absorbance is observed but neither of these features in and of themselves is distinctive of the desired structure. The Raman measurements of the deposited solid showed the most promise of identifying the product so they were examined closely. They clearly show a significant loss of absorption bands (namely the carbonyl peak) and several new peaks appear (not observed in the starting materials) that may be attributable to Sn-O stretching modes (see section 3.2.2). This information indicates that a new product is definitely being formed during the electrochemical synthesis and that it may have the desired stack structures. However, further research is required to reproducibly synthesize these solids and determine their structure conclusively as none of the photophysical measurements that were subsequently performed provided clear evidence of the overall structure.

While the electrochemical synthesis method provided a convenient method for performing a controlled synthesis that could be measured throughout the synthetic process, the product may not provide the desired photo-properties due to the size and orientation of the benzoquinone ligand. For this reason a second synthetic procedure was devised that projected a product that would contain closely bound porphyrins, ideal for TTA, separated only by an oxygen atom. The product of this synthesis showed more distinct changes in its absorption spectrum than the electrochemical product. Shifts in the relative positions of peaks as well as their relative intensities may be indicative of changes to the molecular symmetry or different stabilization effects due to ligation, as seen in the ZnTPP·L case described previously. Unlike the ZnTPP

studies though, with the tin porphyrin case one would not expect the characteristic strong red shift associated with ligation of a porphyrin because the starting molecule is already axially ligated. The changes in the Soret band absorbance were less pronounced but there was a change in the fine structure of the peak due either to a reduction of intensity in the 1-0 B band or because of a shift in the position of the 1-0 band such that it was less easily distinguished from the (0-0) Soret band.

The emission data for the putatitve (SnTPPO)n product was interesting for a number of reasons. First we see a hot band in the S_1 emission spectra of the synthesized product that is much more intense than the small rise visible in the $SnCl_2TPP$ spectrum, though the measurements were taken under identical conditions (with excitation in the Soret band). Further, this hot band (transition from an excited vibrational state) is reproducible and was observed on different days using different samples. In order to observe such a peak, the energy of the vibrational state must be very low as the thermal (Boltzmann) distribution of the population would otherwise dictate a negligible number of molecules in the vibrationally excited state resulting in little or no visible signal. This peak is likely the result of a difference in symmetry between the product and the starting material which allows for transitions from non-totally symmetric vibrational states creating increased peak intensity. This type of change to the symmetry would be expected if the dye monomers had been successfully joined. Further, since a non-structured aggregate tends to promote rapid non-radiative pathways we can be confident that the product of this reaction is not simply an aggregated form of the $SnCl_2TPP$ created during the synthetic procedure as the lifetime data for this product did not show a very significant difference from that of the $SnCl_2TPP$. There was a small difference in the lifetime but the most interesting piece of information was the fact that the S_1 lifetime of both species was significantly decreased when they were excited directly to the Q band as opposed to the Soret band (Table 3.4).

One potential hurdle to the use of the oxygen bridge system that was considered further upon examination of the data obtained for the synthesis was the bond angle between the oxygen atom and the porphyrin macrocycle. Typically a sterically unhindered oxygen would form bonds with an angle equal to ~ 105° which would place the porphyrin rings quite close to each other.

If dimers can be formed with an oxygen atom acting as a bridge they would take on a strained conformation leading to significant wavefunction overlap at one end of the ring and nearly none at the other (figure 4.3).

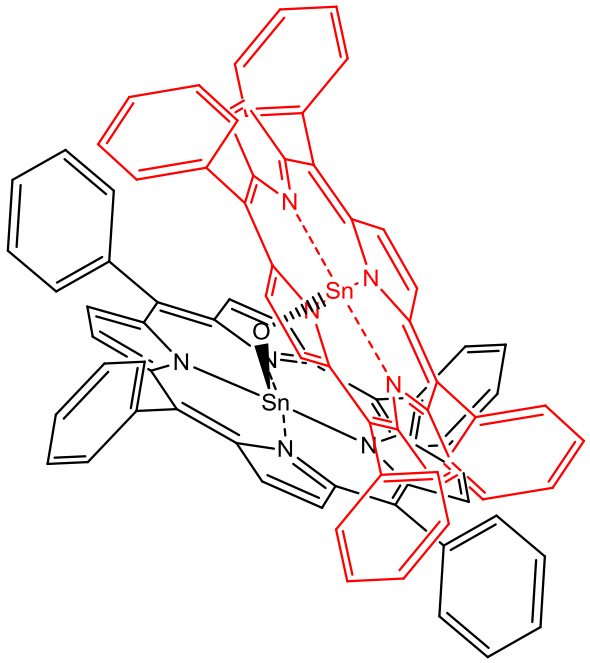

Figure 4.3 Proposed oxygen bridged dimer structure drawn using ChemDraw Pro (version 12.0)

This type of dimer would promote TTA by keeping the dye monomers close to each other but the steric interaction between the two monomers may hinder the formation of such a dimer. Further, this type of stacking would likely prevent the formation of an extended ordered system suitable for attachment to the surface of the TiO_2 nanoparticles.

4.6 Porphyrin viability

The two crucial factors that decide whether a system is viable or not as a DSSC light harvester are the ability to absorb energy and the ability to efficiently transform said energy into electrical potential. The products that were tested in this work do not appear to be an improvement on the simple metallated porphyrin structure as far as photophysical properties go. However, they do provide the potential for creating a tuned dye system that takes advantage of the spectral changes found in these constructs. The fact that nearly every change made to the porphyrins seemed to quench their S_2 lifetime is a fairly major issue. Even if the

stacked porphyrins are able to undergo TTA at an accelerated rate, if the high energy state cannot retain the energy long enough to allow for electron transfer and charge separation then the system will never function efficiently. It is important to note that the information on the charge transfer between porphyrins and axially coordinated ligands may enable us to choose a ligand that will not accept an electron from the metal centre. If this is the case, or if a long-lived charge transfer state capable of transferring energy to the TiO_2 surface is found then the problem of quenching the S_2 state when tethering porphyrins together may be overcome.

5. Summary and future work

5.1 Summary

ZnTPP has been studied in a variety of different environments using various photochemical, spectroscopic and electrochemical methods. Studies on the photophysical effect of linking a nitrogen-containing bidentate molecule to the central Zn atom of the porphyrin were the main object of the research. These ligands were found to have moderate to poor binding affinity for the central metal atom which, coupled with the innate reluctance of the Zn atom to form a six-coordinate structure, led to an inability to form the desired stacked porphyrin structures.

However, this research did yield an understanding of the properties of various linkers, when attached to ZnTPP, and related their photophysical effects to the redox properties of the individual molecules. This in turn allowed for the development of a theory that related the charge transfer dynamics in ligated porphyrin compounds to the redox properties of the linker itself, as compared to the redox properties of the porphyrin. Understanding of these dynamics will make it possible to predict the outcome of future constructs that involve linking molecules to the central metal atoms of porphyrins, thus allowing for less trial and error in planning functional DSSC systems.

$SnCl_2TPP$ was also studied in an effort to create a stacked porphyrin system that would have enhanced TTA characteristics. A number of different synthetic routes and novel synthetic methods for the creation of such a porphyrin stack were examined with a variety of inconclusive results. While each route showed some signs of the desired product the most promising was the oxygen bridged porphyrin stack which also allowed for the closest approach of the individual porphyrins. Each route was studied using multiple methods, predominantly fluorescence and absorbance based spectroscopy, but none showed conclusive evidence that the desired stacked structure had been obtained. This may have been a limitation of the methods used for analysis or simply the result of low yield or unsuccessful synthesis.

5.2 Future work

The experiments and results presented in this work show that much remains to be studied with regard to the basic science of DSSCs before they become a viable energy alternative. This work represents a small foundational piece of these studies which, in the future, can be extended to provide the framework for a more efficient DSSC system. Four experiments that may prove useful in this pursuit are described below.

The stacked of polymeric Sn porphyrins show great promise for serving as an ideal TTA system and further efforts in the synthesis and characterization of such compounds ought to be pursued. It may be necessary to find new synthetic methods for the production of such compounds but an effort to optimize the methods reported herein may prove valuable. Characterization of the products may best be accomplished using a method that is sensitive to the separation of molecules such as NOESY NMR as there are no significant structural changes to the individual porphyrins which makes it difficult to characterise the product using more conventional spectroscopic means.

Once stacked porphyrins have been successfully and reproducibly synthesized there are two important lines of research that must follow; i) TTA efficiency optimization and ii) linking stacks to the semiconductor. The measurement of TTA efficiency should prove to be relatively simple as it can be directly observed by exciting into the S_1 absorbance band and observing whether any S_2 fluorescence is produced. If the stacks do not show significant increases over the performance of individual porphyrins then the synthesis of such constructs may be an unnecessary difficulty in DSSC improvement. However, if they do show increases in TTA it will be crucial to find a method for attaching them onto the surface of the nanocrystalline TiO_2 in such a manner that electron transfer is possible, either through direct physisorption of the porphyrin to the surface or linking the molecule via bridging ligands.

Another potentially useful research pursuit is the building, testing and optimization of a DSSC based on the information gained. This would essentially be a scaling up of the work done on porphyrins which may provide insight on whether or not lab scale techniques can be translated into functional and efficient working cells.

References

1. U.S. Energy Information Administration *International Energy Outlook*, **2011.**

2. Kamat, P.V. *J. Phys. Chem. C*, **2007,** *111(7),* 2834.

3. Graetzel, M. *Nature*, **2001,** *414(6861)*, 338.

4. Luque, A. *J. Appl. Phys.*, **2011,** *110(3),* 031301.

5. Green, M.A.; Emery, K.; Hishikawa, Y. and Warta, W. *Prog. Photovoltaics*, **2010,** *18(5),* 144.

6. Krebs, F.C. *Sol. Energy Mater. Sol. Cells*, **2009,** *93(4),* 394.

7. Clifford, J.N.; Martinez-Ferrero, E.; Viterisi, A. and Palomares, E. *Chem. Soc. Rev*. **2011,** *40(3),* 1635.

8. Balaban, T.S.; Tamiaki, H. and Holzwarth, A.R. *Top. Curr. Chem*. **2005**, *258,* 1.

9. Kalyanasundaram, K. and Graetzel, M. *Curr. Opin. Biotechnol*. **2010,** *21(3),* 298.

10. Wang, X.-F.; Koyama, Y.; Kitao, O.; Wada, Y.; Sasaki, Sl.; Tamiaki, H. and Zhou, H. *Biosens. Bioelectron*. **2010,** *25(8),* 1970.

11. Blankenship, R.E.; Tiede, D.M.; Barber, J.; Brudvig, G.W.; Fleming, G.; Ghirardi, M.; Gunner, M.R.; Junge, W.; Kramer, D.M.; Melis, A.; Moore, T.A.; Moser, C.C.; Nocera, D.G.; Nozik, A.J.; Ort, D.R.; Parson, W.W.; Prince, R.C. and Sayre, R.T. *Science* **2011,** *332(6031),* 805.

12. a) Shockley, W. and Queisser, H.J. *J. Appl. Phys.* **1969**, *32(3),* 510.

    b) Hanna, M.C. and Nozik, A.J. *J. Appl. Phys*., **2006**, *100(7),* 074510.

13. Zhu, X.-G.; Long, S.P. and Ort, D.R. *Annu. Rev. Plant Biol*. **2010,** *61*, 235.

14 Lewis, N.S. *Science* **2007**, *315,* 798.

15. Pizzini, S. *Sol. Energy Mater. Sol. Cells.* **2010,** *94(9),* 1528.

16. Yu, G.; Gao, J.; Hummelen, J.C.; Wudl, F. and Heeger, A.J. *Science* **1995**, *270(5243),* 1789.

17. Gershon, T. *Mater. Sci. Technol.* **2011,** *27(9),* 1357.

18. Dennler, G.; Scharber, M.C. and Brabec, C.J. *Adv. Mater.* **2009**, *21(13),* 1323.

19. Kim, J.Y.; Lee, K.; Coates, N.E.; Moses, D.; Nguyen, T-Q.; Dante, M. and Heeger, A.J. *Science* **2007,** *317(5835),* 222.

20. Hamann, T.W.; Jensen, R.A.; Martinson, A.B.F.; Ryswyk, H.V. and Hupp, J.T. *Energy Environ. Sci.* **2008,** *1(1),* 66.

21. Nakade, S.; Matsuada, M.; Kambe, S.; Saito, Y.; Kitamura, T.; Sakata, T.; Wada, Y.; Mori, H. and Yanagida, S. *J. Phys. Chem. B* **2002**, *106(39),* 10004.

22. Lin, C.C.; Wang, D.Y.; Tu, K.H.; Jiang, Y.T.; Hsieh, M.H.; Chen, C.C. and Chen, C.W. *Appl. Phys. Lett.* **2011,** *98(26),* 263509.

23. A.S.T.M. Standard G173-03, 2008.

24. Qin, C.; Fu, Y.; Chui, C.H.; Kan, C.W.; Xie, Z.; Wang, L. and Wong, W.Y. *Macromol. Rapid Commun.* **2011,** *32(18),* 1472.

25. Muehlbacher, D.; Scharber, M.; Morana, M.; Zhu, Z.; Waller, D.; Gaudiana, R. and Brabec, C. *Adv. Mater.* **2006**, *18(21),* 2884.

26. Huang, F.; Chen, D.; Cao, L.; Caruso, R.A. and Cheng, Y.B. *Energy Environ. Sci.* **2011,** *4(8),* 2803.

27. Ogura, R.Y.; Nakene, S.; Morooka, M.; Orihashi, M.; Suzuki, Y. and Noda, K. *Appl. Phys. Lett*. **2009**, *94(7),* 073308.

28. Uzaki, K.; Pandey, S.S. and Hayase, S. *J. Photochem. Photobiol. A* **2010,** *216(2-3),* 104.

29. O'Regan, B. and Graetzel, M. *Nature*, **1991**, *353(6346),* 737.

30. Toyoda, T.; Sano, T.; Nakajima, J.; Doi, S.; Fukumoto, S.; Ito, A.; Tohyama, T.; Yoshida, M.; Kanagawa, T.; Motohiro, T.; Shiga, T.; Higuchi, K.; Tanaka, H.; Takeda, Y.; Fukano, T.; Katoh, N.; Takeichi, A.; Takechi, K. and Shiozawa, M. *J. Photochem. Photobiol. A* **2004,** *164(1-3),* 203.

31. Kietzke, T. *Adv. OptoElectron.* **2007**, *2007,* 40285.

32. Kroon, J.M.; Bakker, N.J.; Smit, H.J.P.; Liska, P.; Thampi, K.R.; Wang, P.; Zakeerudinn, S.M.; Graetzel, M.; Hinsch, A.; Hore, S.; Wurfel, U.; Sastrawan, R.; Durrant, J.R.; Palomares, E.; Pettersson, H.; Gruszeki, T.; Walter, J.; Skupien, K. and Tulloch, G.E. *Prog. Photovoltaics* **2007**, *15(1),* 1.

33. Kazmerski, L.L. *Renewable Sustainable Energy Rev*. **1997**, *1(1/2),* 71.

34. Anderson, A.Y.; Barnes, P.R.F.; Durrant, J.R. and O'Reagan, B.C. *J. Phys. Chem. C.* **2011,** *115(5),* 2439.

35. Koops, S.E.; O'Regan, B.C.; Barnes, P.R.F. and Durrant, J.R. *J. Am. Chem. Soc.* **2009**, *131(13),* 4808.

36. O'Regan, B.C. and Durrant, J.R. *Acc. Chem. Res.* **2009,** *42(11),* 1799.

37. Listorti, A.; O'Regan, B. and Durrant, J.R. *Chem. Mater.* **2011,** *23(15),* 3381.

38. O'Regan, B.C.; Lopez-Duarte, I.; Martinez-Diaz, M.V.; Forneli, A.; Albero, J.; Morandeira, A.; Palomares, E.; Torres, T. and Durrant, J.R. *J. Am. Chem. Soc.* **2008,** *130(10),* 2906.

39. Peter, L. *Acc. Chem. Res.* **2009,** *42(11),* 1839.

40. a) Suppan, P. *Chemistry and Light*, Cambridge: Royal Society of Chemistry; 1994: p.97-104.

    b) Paddon-Row, M.N. *Adv. Phys. Org. Chem.* **2003,** *38*, 1.

41. Rehm, D. and Weller, A. *Israel J. Chem.* **1970**, *8(2),* 259.

42. Marcus, R. A. *J. Chem. Phys.* **1956**, *24,* 966.

43. Mataga, N.; Taniguchi, S.; Chosrowjan, H.; Osuka, A. and Kurotobi, K. *Chem. Phys. Lett.* **2005**, *403*, 163.

44. Lakowicz J. R. *Principles of Fluorescence Spectroscopy (2nd ed.)*, New York, NY: Kluwer Academic/Plenum Publisher; 1999: p. 367-373.

45. Ishii K. and Kobayashi N. The photophysical properties of phthalocyanines and related compounds. In: Kadish K. M., Smith K. M. and Guilard R. eds. *The Porphyrin Handbook (V.16)*. San Diego, Ca: American Press; 2003: p. 1-42.

46. Goldberg, P.K.; Pundsack, T.J. and Splan, K.E. *J. Phys. Chem. A.* **2011,** *115(38),* 10452.

47. Harriman, A. *J. Chem. Soc. Faraday Trans. 2* **1981**, *77(7),* 1281.

48. Gouterman, M.; Rentzepis, P.M.; Straub, K.D. *Porphyrins: excited states and dynamics.* Washington, DC: American Chemical Society; 1986

49. Dolphin, D. *The Porphyrins (V. 3).* New York, NY: Academic Press; 1978.

50. Lindsey, J.S. *Acc. Chem. Res*. **2010,** *43(2),* 300.

51. Sonogashira, K.; Tohda, Y. and Hagihara, N. *Tetrahedron Letters* **1975,** *16*, 4467.

52. Maeda, C.; Kim, P.; Cho, S.; Park, J.K.; Lim, J.M.; Kim, D.; Vura-Weis, J.; Wasielewski, M.R.; Shinokubo, H. and Osuka, A. *Chem.--Eur. J*. **2010,** *16(17),* 5052.

53. Diev, V.V.; Schlenker, C.W.; Hanson, K.; Zhong, Q.; Zimmerman, J.D.; Forrest, S.R. and Thompson, M.E. *J. Org. Chem.* **2012,** *77(1),* 143.

54. Lash, T.D. *J. Porphyrins Phthalocyanines* **2001**, *5(3),* 267.

55. Chang, J.-C.; Ma, C.J.; Lee, G.H.; Peng, S.M. and Yeh, C.Y. *Dalton Trans*. **2005**, *8,* 1504.

56. Danger, B.R.; Bedient, K.; Maiti, M.; Burgess, I.J. and Steer, R.P. *J. Phys. Chem. A.* **2010,** *114(41),* 10960.

57. Maiti, M.; Danger, B.R. and Steer, R.P. *J. Phys. Chem. A* **2009,** *113(42),* 11318.

58. Marcelli, A.; Foggi, P.; Moroni, L.; Gellini, C.; Salvi, P.R. and Badovinac, I.J. *J. Phys. Chem. A* **2008**, *112(9),* 1864.

59. Yu, H.-Z.; Baskin, J.S. and Zewail, A.H. *J. Phys. Chem. A* **2002,** *106(42),* 9845.

60. Tripathy, U.; Kowalska, D.; Liu, X.; Velate, S. and Steer, R.P. *J. Phys. Chem. A* **2008,** *112,* 5824.

61. Koops, S.E.; Barnes, P.R.F.; O'Regan, B.C. and Durrant, J.R. *J. Phys. Chem. C.* **2010,** *114(17),* 8054.

62. Haque, S.A.; Palomares, E.; Cho, B.M.; Green, A.N.M.; Hirata, N.; Klug, D.R. and Durrant, J.R. *J. Am. Chem. Soc.* **2005,** *127(10),* 3456.

63. Prezhdo, O.V.; Duncan, W.R. and Prezhdo, V.V. *Acc. Chem. Res*. **2008,** *41(2),* 339.

64. Palomares, E.; Martinez-Diaz, M.V.; Haque, S.A.; Torres, T. and Durrant, J.R. *Chem. Commun.* **2004**, *18,* 2112.

65. Singh-Rachford, T.N. and Castellano, F.N. *Coord. Chem. Rev.* **2010,** *254(21-22),* 2560.

66. a) Gouterman, M.; Schwarz, F. P.; Smith, P. D. and Dolphin D. *J. Chem. Phys.* **1973,** *59(2),* 676.

    b) Eastwood, D. and Gouterman, M. *J. Mol. Spectrosc.* **1968,** *30*, 437.

67. Olaya-Castro, A. and Scholes, G.D. *Int. Rev. Phys. Chem.* **2011,** *30(1),* 49.

68. Wardle, B.; *Principles and Applications of Photochemistry.* West Sussex, UK; John Wiley and Sons Ltd.; 2009: p. 78-80.

69. Freed, K.F.; Jortner, J. *J. Chem. Phys.* **1970**, *52,* 6272.

70. Yin, J.; Guo, Q.; Palmer, R.E.; Bampos, N.; Sanders, J.K.M. *J. Phys. Chem. B* **2003,** *107(1),* 209.

71. Kuramochi, Y.; Satake, A.; Itou, M.; Ogawa, K.; Araki, Y.; Ito, O.; Kobuke, Y. *Chem. Eur. J.* **2008,** *14,* 2827.

72. Camus, J.; Aly, S.M.; Stern, C.; Guilard, R.; Harvey, P.D. *Chem. Commun.* **2011,** *47,* 8817.

73. Litvinov, A.L.; Konarev, D.V.; Kovalevsky, A.Y.; Neretin, J.S.; Coppens, P.; Lyubovskaya, R.N. *Cryst. Growth Des.* **2005,** *5(5),* 1807.

74. a) Irvine, M.P.; Harrison, R.J.; Beddard, G.S.; Leighton, P.; Sanders, J.K.M. *Chem. Phys.* **1986,** *104(2),* 315.

b) Hunter, C.A.; Sanders, J.K.M.; Stone, A.J. *Chem. Phys.* **1989,** *133(3),* 395.

75. Yeow, E.K.L. ; Steer, R.P. *Phys. Chem. Chem. Phys.* **2003,** *5,* 97.

76. Kubista, M.; Sjoback, R.; Erikkson, S.; Albinsson, B. *Analyst.* **1994**, *119,* 417.

77. Andrew, E.R. *Progress in Nucl. Mag. Res. Spect.* **1971**, *8(1),* 2.

78. Davison, J.B.; Wynne, K.J. *Macromolecules.* **1978**, *11(1),* 186.

79. Joyner, R.D.; Kenney, M.E. *Inorg. Chem.* **1962**, *1,* 717.

80. Liu, X.; Tripathy, U.; Bhosale, S. V.; Langford, S. J.; Steer, R. P. *J. Phys. Chem. A* **2008**, *112*, 8986.

81. Tabata, M.; Nishimoto, J. Equilibrium Data of Porphyrins and Metalloporphyrins. In: Kadish K. M., Smith K. M. and Guilard R. eds. *The Porphyrin Handbook (V.9)*. San Diego, Ca: American Press; 2003: 263

82. Stammreich, H.; Teixeira Sans, Th. *J. Chem. Phys.* **1965**, *42(3)*, 920.

83. Aggarwal, R.C.; Singh, P. P. *J. Inorg. Nuc. Chem.* **1966**, *28(8)*, 1655.

84. Nappa, M. and Valentine, J.S. *J. Am. Chem. Soc.* **1978,** *100(16)*, 5075.

85. DiMagno, S.G.; Wertsching, A.K. and Ross C. R. *J. Am. Chem. Soc.***1995,** *117(31)*, 8279.

86. Sugunan, S.K.; Tripathy, U.; Brunet, S.M.K.; Paige, M.F.; Steer, R.P. *J. Phys. Chem. A* **2009,** *113,* 8548.

87. Kowalska, D.; Steer R.P. *J. Photochem. Photobiol. A* **2008,** *195,* 223.

88. Ou, Z.; E, W.; Zhu, W.; Thordarson, P.; Sintic, P.J.; Crossley, M.J.; Kadish, K.M. *Inorg. Chem.* **2007,** *46*, 10840.

APPENDICES

Appendix A: Pyrazine-ZnTPP ligation spectra

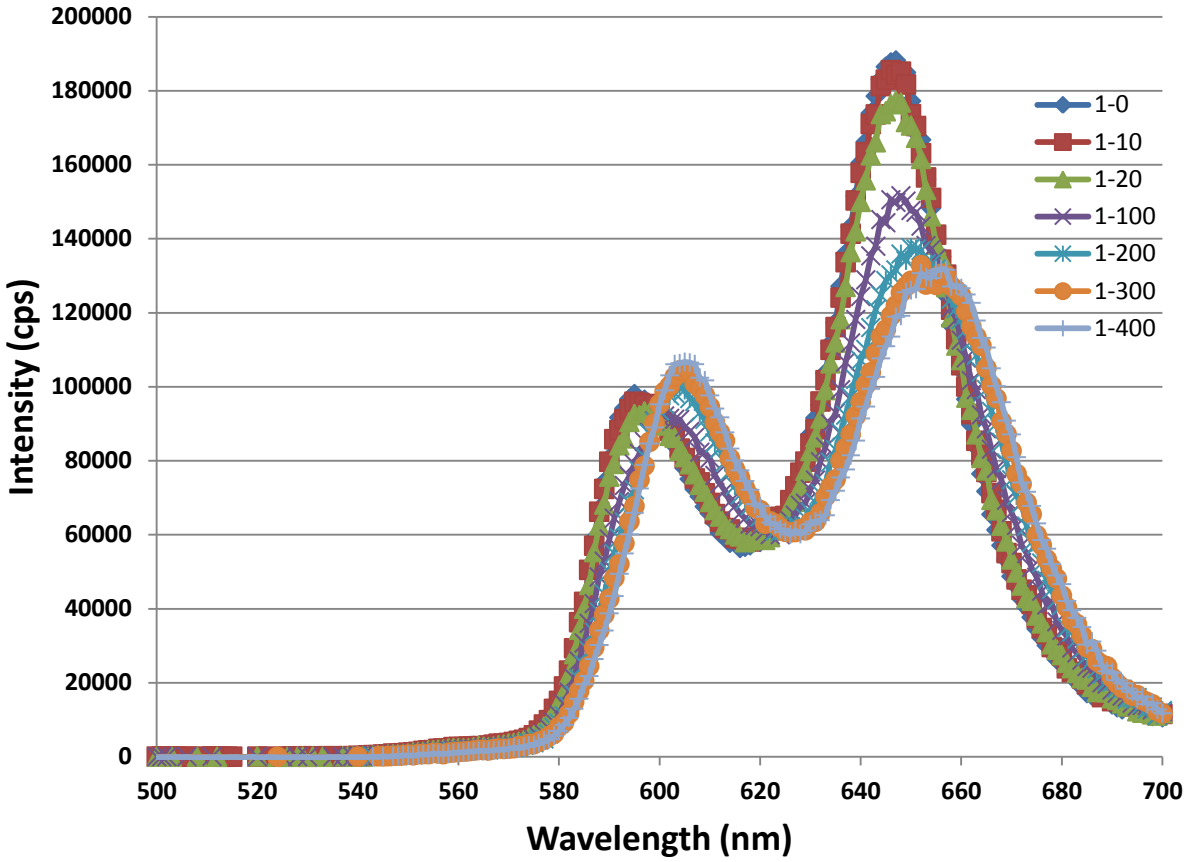

Figure A.1: ZnTPP S_1 emission in aerated toluene with varying concentrations of pyrazine.

λ_{ex} = 405 nm

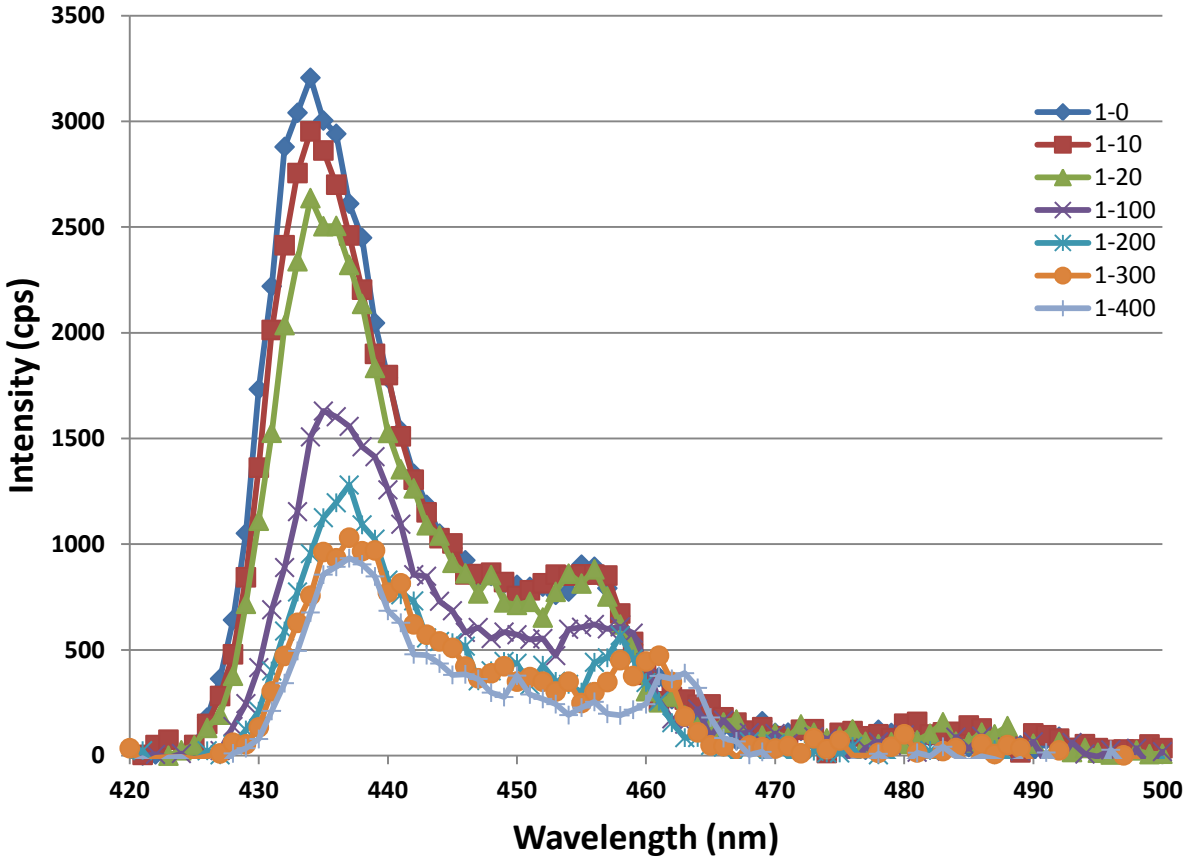

Figure A.2: ZnTPP S_2 emission in aerated toluene with varying concentrations of pyrazine. λ_{ex} = 405 nm

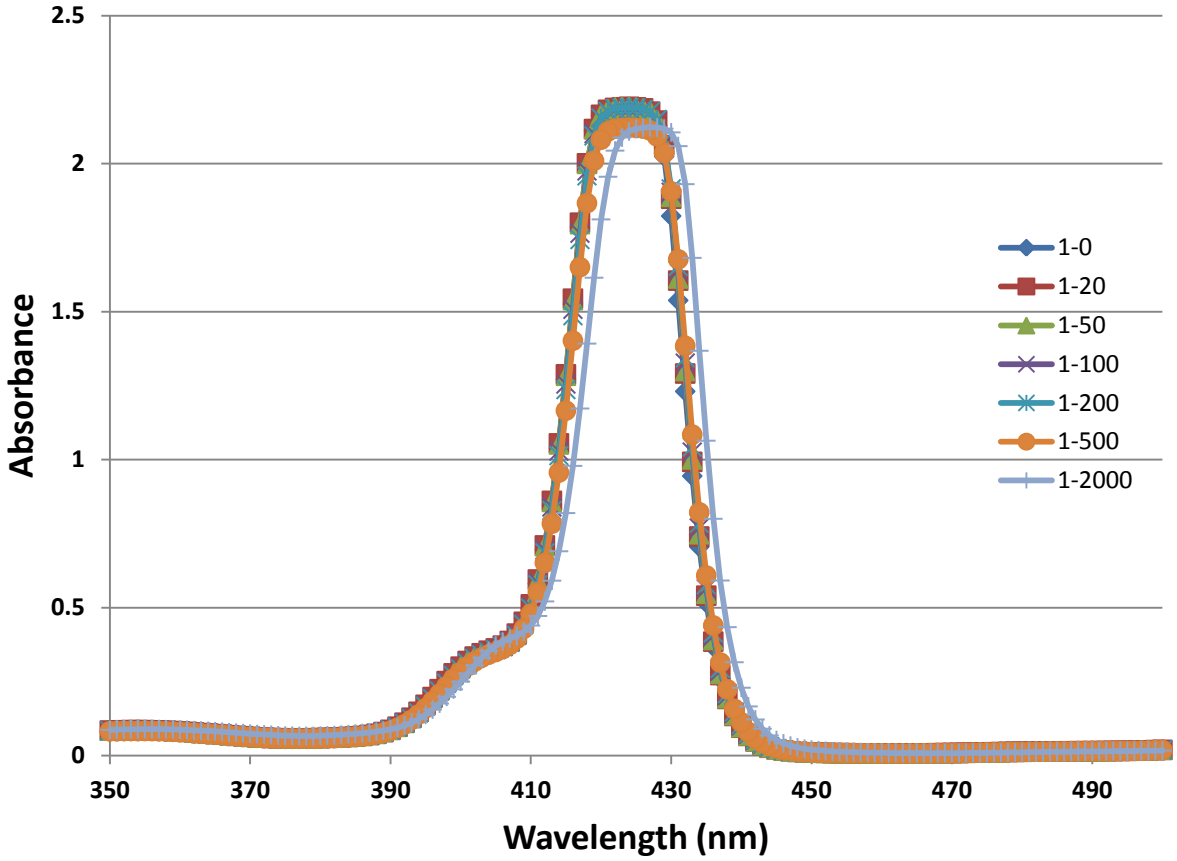

Figure A.3: ZnTPP S_2 absorbance in aerated toluene with varying concentrations of pyrazine.

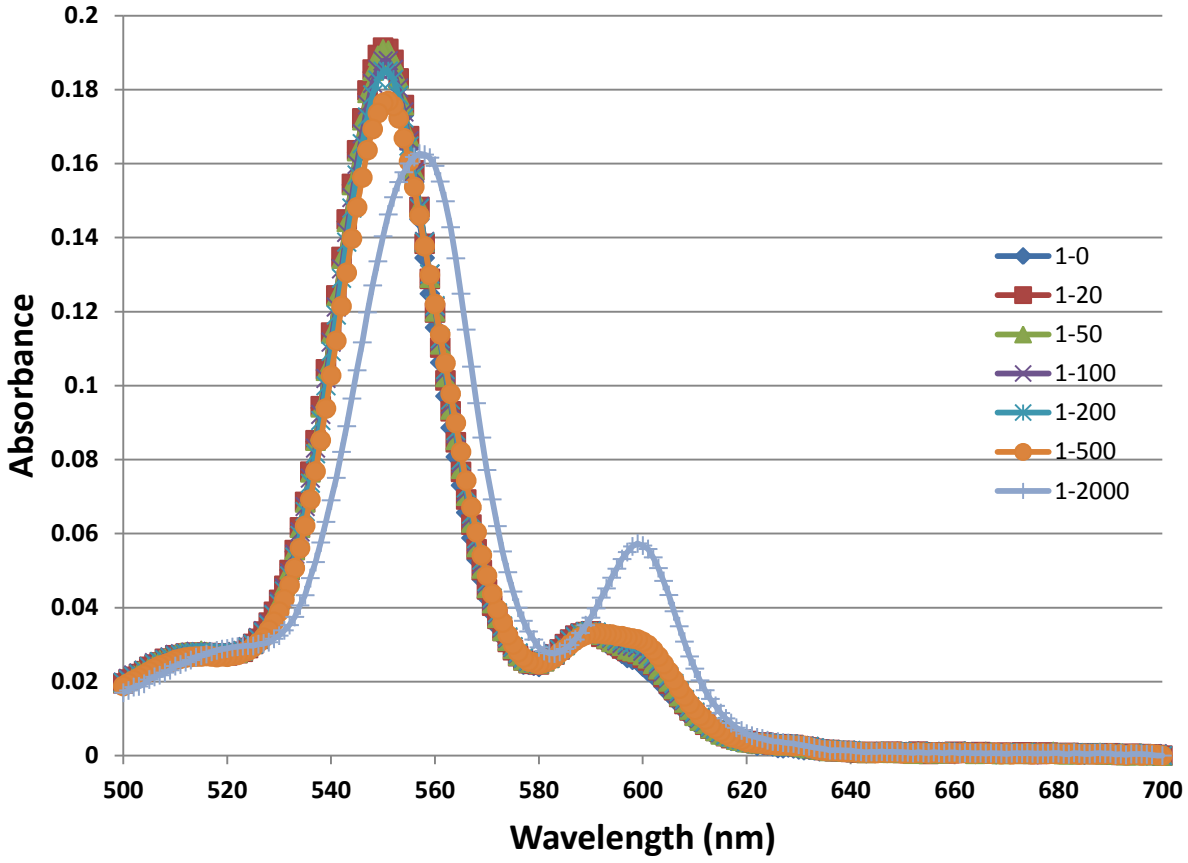

Figure A.4: ZnTPP S_1 absorbance in aerated toluene with varying concentrations of pyrazine.